The Evaluation of Sentinel-2's Potential to Identify and Map the Geology of the Vredefort Dome

By: Mpho Bogatsu (448251)
Supervisor: Prof. Fethi Ahmed

Submitted in partial fulfilment of the requirements for the degree of MSc in GIS and Remote Sensing

School of Geography, Archaeology and Environmental Studies Faculty of Science
University of the Witwatersrand, Johannesburg

September 2019

Declaration

"I, the undersigned, hereby declare that the research report submitted for the degree Masters of Science in Geographic Information Systems and Remote Sensing, at the University of the Witwatersrand, Johannesburg, is my own original work and has not been previously submitted to any other institution of higher education. I further declare that all sources cited or quoted are indicated and acknowledged by means of a comprehensive list of references."

____________________________ ____________________________

(Signature of candidate) (Date)

This study is dedicated to:

My loving mother Hlupi Jeanette Kate Bogatsu

whose prayers and support have seen me

through the toughest parts of this degree.

Acknowledgements

I, the author wish to express my sincere gratitude and appreciation to:

- God for giving me the strength to complete this research project.
- My mother, Hlupi Bogatsu, for her never-ending support, encouragement and prayers throughout the course of this research project.
- My project supervisor, Prof. Fethi Ahmed, for his continuous constructive criticism, endless support and guidance throughout this entire process.
- The South African National Space Agency (SANSA) for providing me with the funding to pursue this degree.
- Dr Elhadi Adam, Dr Jolene Fisher and Prof. Barend Erasmus for their constructive criticism on my initial research proposal presentation.
- Prof. Rodger Gibson for sharing his expertise and being readily available for consultations.
- Dr Solomon Tesfamichael, from the University of Johannesburg, for lending me the spectroradiometer I required to capture the spectral signatures of the rocks and for offering his expert advice when required.
- The European Space Agency (ESA) for making the necessary Sentinel data freely available.
- Dr Stefania Merlo for her support as the Master's course coordinator and Research Methods in GIS and RS (GEOG 7045) lecturer. The lessons learnt during her course really aided in the compilation and completion of this research project.
- Lastly, to all my fellow MSc students who played a role in helping me with some of the GIS and Remote Sensing techniques used in this research project.

Abstract

Remote sensing has become one of the fastest emerging sciences due to its earth observation capabilities. Fields such as mineral exploration, have in recent years benefited from the help of remote sensing spectroscopy. This is because every rock type has a unique spectral response to electromagnetic radiation due to their varying crystal structures and chemical compositions, which can be picked up in satellite imagery and be used in the identification and mapping of exposed rock types. The main problem is that not all sensors are capable of accurately detecting such features, therefore it becomes important to evaluate the potential of different sensors to determine which can best identify the surface geology of any given environment.

This study focuses on the surface geology of the two-billion-year-old meteoritic collision that occurred in the Vredefort Dome, South Africa. This is mainly due to the fact that the geology in this region possesses unique traits such as a superimposed rock stratigraphy that has never been analysed using remote sensing spectroscopy. Seven dominant rock types, namely, granite gneiss, basalt, quartzite, meta-ironstone, banded iron formation (BIF), metadolerite and metapelite were sampled from the Donkervleit region of the Dome and their spectral reflectances were measured using a spectroradiometer in the field. Their absorption features were also analysed before and after continuum removal was applied to the spectra using ENVI software.

Results showed that there were subtle, yet distinct, spectral differences between all the rock types that occurred in the Donkervleit region of the Dome but the biggest difference between the rock types could be observed between the quartzite and basalt because of their non-overlapping mineral compositions. The variability of spectral characteristics within rock types was attributed to differences in rock texture and grain size, and the spectral differences between the rock samples were attributed primarily to differences in mineral composition. The rock identification capabilities of Sentinel-2 imagery were also assessed and it was found that only a 79% accuracy could be achieved through this method; proving that Sentinel-2 is not that efficient at mineral identification when compared to other multispectral sensors such as Aster and Landsat which have been known to produce accuracies between 82% - 92%.

Keywords: Multispectral, Sentinel-2, Spectroscopy, Vredefort Dome, Geological Mapping

Table of Contents

List of Figures

List of Tables

List of Acronyms and Abbreviations

ASTER	Advanced Spaceborne Thermal Emission and Reflection Radiometer
BIF	Banded Iron Formation
ESA	European Space Agency
GIS	Geographic Information Systems
IFOV	Instantaneous Field of View
MNF	Minimum Noise Fraction
MSS	Multispectral Sensor
NIR	Near Infrared
RF	Random Forest
ROI	Regions of Interest
RS	Remote Sensing
SAM	Spectral Angle Mapper
SFF	Spectral Feature Fitting
SWIR	Shortwave Infrared
UNESCO	United Nations Educational, Scientific and Cultural Organization
USGS	United States Geological Survey
UTM	Universal Transverse Mercator
VNIR	Visible Near Infrared
WSG	World Geodetic System
XRF	X-Ray Fluorescence

Chapter 1: Introduction

1.1 Background

Over the last two decades, remote sensing has become crucial to many disciplines, one of which is mineral exploration (Sabins, 1999; Gupta, 2013). Geological recognition and mapping are some of the primary tasks of geologically oriented remote sensing. Remote sensing applications are very useful especially in cases where extreme environmental conditions make it difficult to collect *in situ* data (Pour *et al*., 2018).

Geological mapping from remote sensing data implies a typical methodology comprising different levels of analysis: image calibration, correction for atmospheric effects, image analysis (statistical and/or deterministic), field verification, and final interpretation (Mustard and Sunshine, 1999). Knowledge of the mechanisms of interaction between electromagnetic radiation and surface materials is instrumental in fulfilling all these steps. In particular, in the optical range, the most relevant surface property for geologic remote sensing is the reflectance property (Mustard and Sunshine, 1999).

The spectral intensity of solar radiation reflected by any natural surface is influenced by the physical and chemical properties of the material (Mustard and Sunshine, 1999). Various electronic and molecular processes arise from the interaction between incident light and rock minerals (Tempfli *et al.*, 2009; Gupta, 2013). Every rock type has a unique spectral response to electromagnetic radiation due to their varying crystal structures and chemical compositions, which can be picked up in satellite imagery and be used in the identification and mapping of exposed rock types (Tempfli *et al*., 2009; Gupta, 2013).

In the 0.4-2.5 μm range, the spectral features in reflectance spectra of rocks are due to high-energy electronic processes at short wavelengths and to atomic and molecular vibration processes at longer wavelengths (Hunt and Salisbury, 1970; Hunt *et al*., 1973; Hunt, 1980; Crowley *et al*., 2003). In the VNIR range, spectral features of the most common rock-forming minerals are stable and can be used to identify the mineral phases (Crowley *et al.*, 2003). Because rocks are formed of minerals, the relative abundance of their mineral constituents will be the main factor controlling their spectral signature. Other important factors are structure, texture and the state of alteration of the rock surface (Sabins, 1999; Crowley *et al.*, 2003).

The collection of reflectance spectra of different materials is finalized in the production of a spectral library. Generally, the main purpose of a spectral library is to feed a remote sensing data analysis system with the ground truth needed to perform image calibration and reliable geologic interpretation (Clark *et al.*, 2007). Although many spectral libraries have been published, they have a limited use in geological mapping, especially with low spectral resolution data, since they are usually composed of laboratory measurements of mineral samples (usually pulverized). A more practical approach consists of collecting rock spectra in the field or in the laboratory over the actual reflecting surfaces. Such spectra yield a very accurate ground truth for the application of both statistical and deterministic techniques of image analysis. In the most favourable cases, a few well-chosen rock spectra will provide all the analysis needed for geological mapping of a large area such as the Vredefort Dome.

This study assesses the rock identification, as well as the mapping capabilities of high-resolution multispectral Sentinel-2 data in conjunction with field and laboratory obtained data. The region of interest is the Vredefort Dome, which is in the South African province of Free State (Gibson and Reimold, 2008). This structure is a result of a two-billion-year-old meteoritic collision that occurred at very high speeds causing the rocks below the impact site to rebound and form a dome (Gibson and Reimold, 2008). Its geological history and unique traits such as its superimposed rock stratigraphy are what make the area the perfect candidate for field-based analysis and remote geological mapping.

1.2 Research Rationale

This research was deemed worthy of investigation for a number of reasons but mainly because even though there have been studies of a similar nature done in other parts of the world such as Nevada and the south-east parts of Spain (Kruse, 2012; Van der Meer *et al.*, 2014), none have been applied to the South African geological context, therefore, making it crucial to apply well-documented techniques in mapping geological structures in South Africa especially in the geologically important area of the Vredefort Dome.

Also, according to literature, Sentinel sensors were created mainly for vegetation identification purposes (Frampton *et al.*, 2013; Van der Meer *et al.*, 2014; Immitzer *et al.*, 2016), so it seemed worthwhile to investigate its potential in identifying other surface objects such as rocks and minerals because the identification of different rock types using both field and laboratory spectroscopy, in conjunction with multispectral remote sensing imagery, could potentially reduce the time and costs involved in mineral exploration and also drastically increase the likelihood of finding hidden mineral and ore deposits which would greatly benefit the South African economy which is currently heavily dependent on the mining sector.

The abovementioned process also requires the creation of a spectral library which will play a significant role as a reference database consisting of signatures against which spectra in the imagery can be compared. The creation of such a database is crucial because, as is, most spectral libraries that exist are mainly owned and used by private and corporate entities, and as such are not readily available for public consumption or academic pursuits.

1.3 Research Question

Can the surface geology of the Vredefort Dome be accurately detected and mapped out using a multispectral sensor such as Sentinel-2?

1.4 Aims

The aims of this project were firstly to assess how accurate and useful spectral signatures are in geological mapping. Secondly, it was to assess if the surface geology of a certain region could be mapped out using a multispectral sensor such as Sentinel-2 in a geologically diverse area such as the Vredefort Dome.

1.5 Objectives

The specific objectives of the study were to:

- Capture and analyse the spectral signatures of some of the rock samples found in the study area by using a spectroradiometer.
- Use ENVI to process the collected spectral signatures in order to create a spectral library of the rocks in the study area.
- Identify and map the different rock types that make up the study area.
- Assess how accurately Sentinel-2 was able to map out the geology of the study area by comparing the results to other literature.

1.6 Chapter Sequence

This document consists of six chapters. The first chapter provides an outline of the background of the study and also highlights the aims and objectives of the study to be achieved. The second chapter provides a detailed review of the literature related to this investigation. Chapter three provides the necessary background information about the study area and then outlines the materials used alongside the methods employed to acquire and process the relevant data. All the results of this study are then presented in chapter four and discussed in chapter five. Chapter six concludes the study, notes some of its limitations and provides relevant recommendations.

Chapter 2: Literature Review

2.1 Introduction

Earth observations through the discipline of Remote Sensing has made the world at large more curious about their surroundings. Mineral exploration has been for so long an area which required a tedious amount of time and work in the field but with the help of remote sensing spectroscopy this no longer needs to be the case.

While there might be a lot of research on the identification of lithological characteristics using spectral remote sensing technology (Kruse, 2012; Van der Meer *et al.*, 2014; Yokoya *et al.*, 2016), literature suggests that there is a lack of information on this topic with reference to the African continent. Thus, this becomes of academic importance because Africa (South Africa in particular) has an abundance of unique geology worth well documenting.

In order to fully understand the scope of this project, this literature review will discuss the spectral reflectance of rocks and what role remote sensing plays in this. Also, literature highlighting the use of spectral signatures in mineral identification as well as the key methods for classifying multispectral imagery is included. Furthermore, this review will take a look at a general overview of some of the advantages and disadvantages of spectroscopy, with respect to some of the most widely used technology, and the techniques used in previous studies which could be utilized in this present study.

2.2 Multispectral Remote Sensing

Multispectral remote sensing is centred around the acquisition of image data related to the Earth's surface, which is obtained across a wide range of wavelengths (Kumar *et al.*, 2013; Yokoya *et al.*, 2016). Therefore, it can be deduced that different objects on the Earth's surface are able to reflect and absorb light of different wavelengths with varying intensity which allow us to differentiate between objects by using their unique spectral reflectance signatures. For many decades, multispectral remote sensing data has been used to map out various Earth observations such as temporal changes and continuous environmental impact changes due to events such as deforestation and mining activities (Kumar *et al.*, 2013; Yokoya *et al.*, 2016).

2.2.1 Spectral Reflectance of Rocks

Spectral reflectance is the efficiency by which a material reflects energy as a function of wavelength (Tempfli *et al.*, 2009). What this means is that measurements of samples such as rocks, can be obtained with very little preparation or manipulation of the sample, which is why reflectance spectroscopy is considered as one of the most suitable techniques for *in-situ* sample analysis (Tempfli *et al.*, 2009).

The spectra of rocks rely heavily upon the spectra of the constituent minerals as well as their textural properties such as grain size and mineral packing order (Clark, 1999). In areas which experience semi-arid to arid conditions, the spectral reflectance curves of rocks and minerals can be used to directly interpret and analyse the lithology and hydrothermal alteration in the region of interest, however, this must be done with caution because weathering can lead to spectral measurements that are significantly from the results obtained from the unweathered parent rock which can construe the final results of the analysis (Clark, 1999). Also, the spectra of rocks are drastically compromised by opaque minerals because such minerals have a tendency to decrease the total reflectance from the rocks as well as their reflectance spectra (Clark, 1999).

2.2.2 The Infrared Region

There are a number of spectral wavelength regions but the one that has been recognised as the most effective at mineral identification is the infrared region due to the fact that most rocks consist of target minerals that have electronic and vibrational characteristic features that can be identified in this region (Clark, 1999; Stephens *et al.*, 2009). To be able to cover the full extent of the infrared region, a series of spectroradiometers fitted with a changing illumination source for detecting the variations in reflectance measurements across each wavelength range would be required but if the region of spectrum can be narrowed down by focusing only on a specific type of samples then this is not really necessary. For the purposes of this study, we will focus only on metamorphic rocks since those are the types of rocks present in the study area.

Literature suggests that the infrared region of the spectrum between 0.4 µm and 2.5 µm can provide information about the mineralogical composition and absorption features of most metamorphic rock types due to its ability to detect hydroxyl and carbonate bond related vibrations which allow it to identify and discriminate between carbonates, micas, chlorite and clay minerals (Clark 1999; Crowley *et al.*, 2003; Stephens *et al.*, 2009; Skok *et al.*, 2010). The aforementioned information therefore implies that hyperspectral data would be more efficient than multispectral data at determining mineral composition, but this study still chooses to focus on multispectral data because of the reasons stated in the research rationale (section 1.2).

2.2.3 Absorption features

Absorption features are usually associated with transition metal ions but can also be linked to the vibrational processes of H_2O and OH- molecules (Van der Meer and De Jong, 2011). These molecules are formed by strings of bonded atoms and they experience vibrations which are generated when they absorb energy particularly in the ground state (Van der Meer and De Jong, 2011). The frequency and intensity of the vibrations are merely dependent on the strength of the strings and because it takes very little energy to cause a vibration, that is why most distinctive absorption features occur at high wavelengths such as in the infrared region between 0.4 µm up to 2.5 µm (Van der Meer and De Jong, 2011).

In order to characterize an absorption feature, one must analyse its position, shape, width, depth and whether it's symmetrical or asymmetrical. This is because these characteristics are usually unique to the chemical structure as well as the crystal structure in which the absorbing element can be found and can therefore be directly related to the mineral composition of a specific rock type (Van der Meer and De Jong, 2011).

2.2.4 The use of spectral signatures in mineral identification

The concept of spectral signatures is based on the idea that a given material has a spectral reflectance which distinguishes it from other materials due to its ability to reflect and absorb light differently at different wavelengths (Kruse, 2012; Kumar *et al.*, 2013; Ngcofe and Niekerk, 2016). This means that the success of our differentiation is determined by the type of sensor we choose to use as well as the materials being analysed (Shaw and Burke, 2003).

There are three main procedures that can be used to obtain the spectral signatures of natural surfaces (Bertel *et al.*, 2006; Anbazhagan and Arivazhagan, 2010). Firstly, spectral signatures can be obtained in the open field, under natural conditions and directly from the targeted outcrops. Secondly, these procedures can also be carried out under controlled field conditions, where the samples may be removed from their original setting and taken to a location which mimics their original setting but allows for better assessment either because of the improved stability of the instrument being used and/or due to being able to measure the spectra under clear sunlight. The third manner in which spectral signatures can be obtained is in a laboratory, where there is optimal light and no atmospheric interference (Bertel *et al.*, 2006; Anbazhagan and Arivazhagan, 2010).

Unfortunately, the problem is not as simple as it may appear since other factors besides the sensor play a role, such as solar angle, view angle, surface wetness as well as background and surrounding material (Tempfli *et al.*, 2009). Also, no matter the scientific application, be it mineral exploration, agriculture or urban development, all of them require ground truth signatures collected in the field and then processed and normalized using continuum removal techniques which are imperative in extracting the necessary diagnostic absorption features from the collected reflectance spectrum (Clack, 1999; Van de Meer, 2000). This data is then indexed in spectral libraries in order to execute thorough analysis (Clark *et al.*, 2007; Ngcofe and Niekerk, 2016). For instance, spectra of vegetation are influenced by such a wide range of environmental conditions that it makes it difficult to adequately represent this variability without the collection of site-specific field spectra (Tempfli *et al.*, 2009).

Minerals and rocks also have unique spectral characteristics due to their varying chemical makeup and water content that may be difficult to distinguish without ground truth data (Tempfli *et al.*, 2009). For example, chemically bound water can cause several diverse rock types to appear to have similar features on satellite imagery which can only be remedied by using remote sensing software such as ENVI to compile a spectral library from the signatures collected in the field (Tempfli *et al.*, 2009; Amrutkar *et al.*, 2016). An example of the spectral signature of certain minerals can be seen in the graph below (Figure 1).

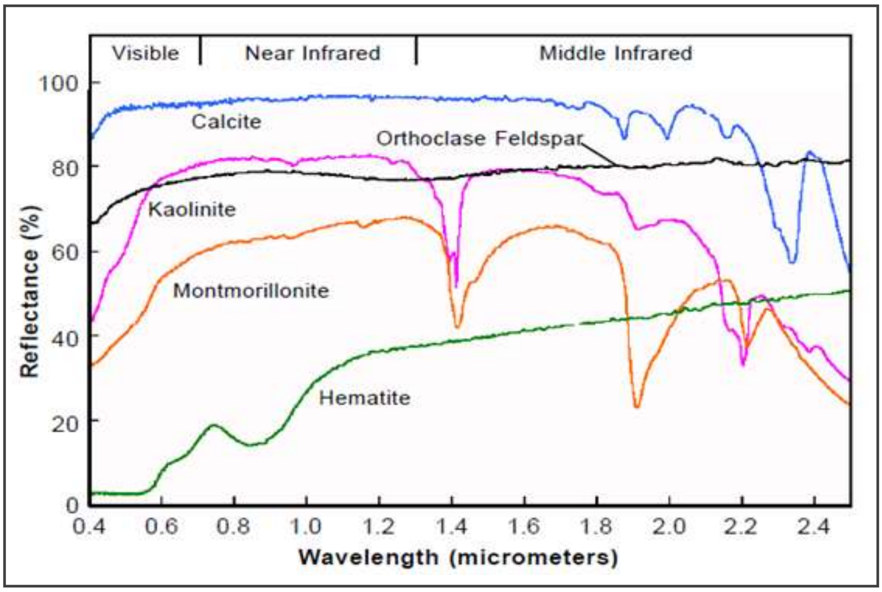

Figure 1: Spectral Signatures of Certain Minerals (Smith, 2012)

2.2.5 Spectral Libraries

A spectral library, by definition, is a catalogue/database that contains the spectral signatures of any material on the Earth's surface (Borengasser *et al*., 2007). Many researchers have dedicated their time to the collection of the spectral signatures of various objects in pursuits of cataloguing them in spectral libraries. These libraries are necessary because apart from being an effective way of recording the spectral signatures of the particular samples of interest, they also provide a source of reference spectra that can be used in the interpretation of multispectral as well as hyperspectral images (Borengasser *et al*., 2007; Qaid and Basavarajappa, 2008).

Pre-existing spectral libraries such as the USGS High Resolution Spectral Library and the ASTER Spectral Library are already widely used for rock/mineral identification but they do not possess the spectral signatures for every rock type in the world, therefore, some researchers are still burdened with the task of having to create their own spectral libraries in order to identify the objects under investigation (Borengasser *et al*., 2007; Clark *et al.*, 2007;

Baldridge *et al.*, 2009). Software packages such as ENVI and SpectraST have built-in processors that can be used to analyse spectral data and create spectral libraries.

2.2.6 Different Algorithms Used in Spectroscopy

Machine learning refers to a set of algorithms that can receive input data and use statistical analysis to predict an output value that is accurate and useful in assessing scientific applications such as geological classification (Parakh *et al.*, 2016). Researchers such as Yu *et al* (2012) and Parakh *et al* (2016) have attempted to find the best methods to improve the classification results for lithological mapping. Cracknell and Reading (2014) compared five machine learning algorithms and their responses to variations in spatial information. This study showcased some of the pros and cons of all the methods explored. One of the key findings was that Random Forest (RF) was one of the best methods that could be used for geological classification, mainly because it is not sensitive to noise and overfitting of training data (Cracknell and Reading, 2014; Parakh *et al.*, 2016).

Other algorithms worthy of mention are Spectral Angle Mapper (SAM) and Spectral Feature Fitting (SFF). The Spectral Angle Mapper technique calculates the spectral angle between the reference spectrum and the pixel spectrum; the smaller the angle the greater the similarity (De Carvalho and Meneses, 2000; Girouard *et al*., 2004). SAM is unaffected by solar illumination and shadow effects. Hence, SAM is preferable for lithological discrimination as the orientation of different rock types may be different with respect to solar illumination and may cause a shadow effect (De Carvalho and Meneses, 2000). SAM calculates the spectral angle by taking the arc-cosine of the dot product between the test spectrum's "t" to a reference spectrum "r" (De Carvalho and Meneses, 2000; Ngcofe and Niekerk, 2016).

Spectral Feature Fitting, on the other hand, is a detection algorithm that matches the library and image spectra (Borengasser *et al*., 2007). It is done by comparing specific absorption features of image spectra with library spectra (Borengasser *et al*., 2007). This algorithm measures two things in particular: shape and depth (Borengasser *et al*., 2007).

One of the main objectives of this study is to use field-based and satellite-obtained results to identify and map the geology of the region of interest. According to literature, the Spectral Angle Mapper (SAM) algorithm will be best to map the given terrain because as previously mentioned SAM is not affected by direct sunlight or shadow effects that can be caused by the varying topography found in the study area (De Carvalho and Meneses, 2000; Ngcofe and Niekerk, 2016).

2.3 Sentinel-2

The ESA's Sentinel-2 has recently become one of the most common multispectral imagers used after the likes of NASA's Landsat (Kumar *et al.*, 2013; Van der Meer *et al.*, 2014; Yokoya *et al.*, 2016). Sentinel-2 is a 13-band imaging instrument with a spectral range from visible to short wave infrared (SWIR). It is commonly used for monitoring a variety of landscape scale properties such as forest monitoring, land cover change detection, and natural disaster management (Kumar *et al.*, 2013). The sensor characteristics of Sentinel-2 have been summarised in Table 1.

As previously mentioned, the spectral reflectance curves of most metamorphic rocks exhibit absorption features between 0.4 µm and 2.5 µm, which are the ranges for water and hydroxyls (Crowley *et al.*, 2003; Skok *et al.*, 2010). The central wavelengths and resolutions of each Sentinel-2 band are given below in Table 2.

As can be seen in Figure 2, in order to comply with the criteria for metamorphic rocks mentioned above, bands 3, 4, 8, 11 and 12 will be used (Kruse, 2012; Ge *et al.*, 2018). Bands 5-7 and band 8A do fall within the required range but were not selected because they are Vegetation Red Edge bands which are best utilized for vegetation detection (Drusch *et al.*, 2012). Band 10 was also excluded because of the fact that this band's purpose is for identifying cloud cover and since the image used was purposefully chosen because of its minimal cloud cover and it was also atmospherically corrected to minimize any atmospheric interferences, this band's use became null and void (Drusch *et al.*, 2012).

Table 1: Sensor Characteristics of Sentinel-2 (Drusch et al., 2012)

Launched	June 2015
Sensor Type	High Resolution Multispectral
Spectral Range	0.4 - 2.5 µm
Spectral Bands	13
Spatial Resolution	60 m, 20 m, 10 m
Sensor Altitude	786 km
Pushbroom Instrument	Yes
Swath Width	290 km
Spectrometers	(VNIR) spectrometer (0.4 - 1.0 µm)
SWIR Spectrometer	Approximately 0.9 – 2.5 µm

Table 2: Spectral Characteristics of Sentinel-2 (Kaplan and Avdan, 2017)

Sentinel-2 Bands	**Central Wavelength (µm)**	**Resolution (m)**
Band 1 – Coastal Aerosol	0.443	60
Band 2 – Blue	0.490	10
Band 3 – Green	0.560	10
Band 4 – Red	0.665	10
Band 5 – Vegetation Red Edge	0.705	20
Band 6 – Vegetation Red Edge	0.740	20
Band 7 – Vegetation Red Edge	0.783	20
Band 8 – NIR	0.842	10
Band 8A – Vegetation Red Edge	0.865	20
Band 9 – Water Vapour	0.945	60
Band 10 – SWIR - Cirrus	1.375	60
Band 11 – SWIR	1.610	20
Band 12 – SWIR	2.190	20

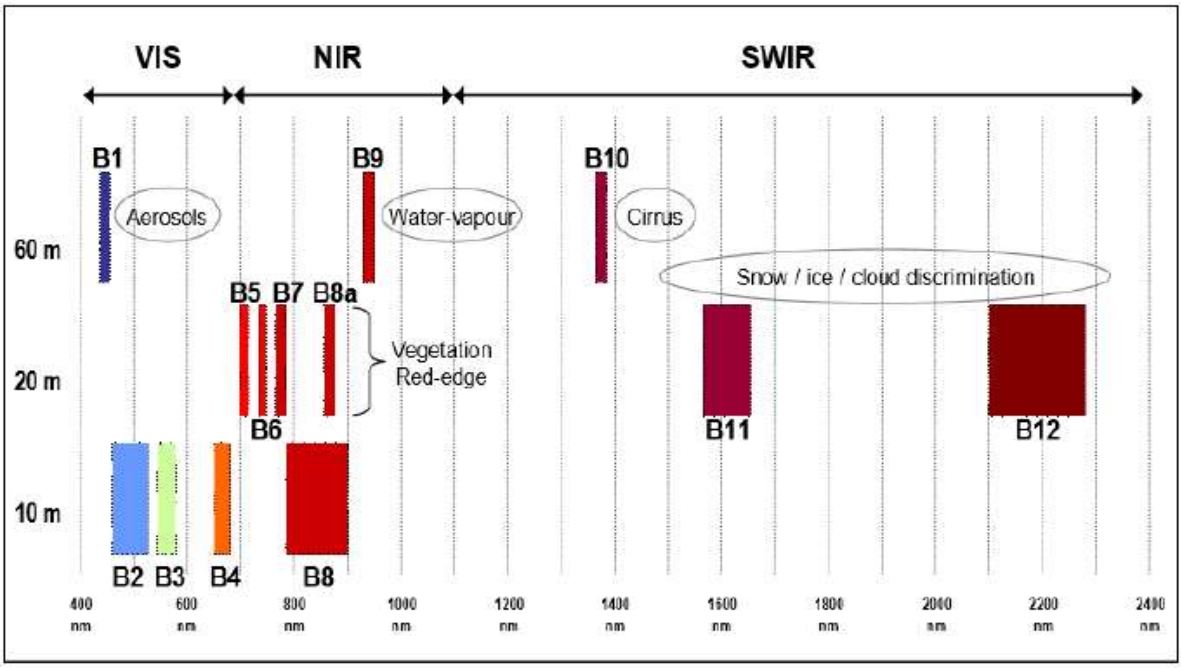

Figure 2: Sentinel-2 Bands and Their Corresponding Spectral Ranges (Martimort et al., 2012)

2.4 Advantages and Disadvantages of Spectroscopy

The field of spectroscopy has its fair share of advantages and disadvantages. Amongst the biggest advantages of spectroscopy is the ability to save time and reduce costs through the instruments used in the field. With that said, those very instruments, such as the ASD FieldSpec Pro often require favorable weather conditions, meaning, if there is cloud coverage or no direct sun light present, the performance of spectroradiometers deteriorates resulting in spurious results (Tempfli *et al.*, 2009).

Also, some spectroradiometers, such as the GER IFOV, have very small and fixed dimensions (8 cm x 4 cm), which are not always effective when taking sample measurements (Toselli and Bodechtel, 1991). This, however, can be counteracted by using instruments such as the FieldSpec Pro FR which have an IFOV that can reach a radius of 20 cm, which can allow for a better averaging of spectral signatures which is particularly beneficial when used in conjunction with remote sensing imagery because it can produce results with a higher accuracy (Kuester *et al.*, 2001). Likewise, the speed at which the FieldSpec Pro FR operates is also marginally faster than other spectroradiometers on the market which is ideal for calibration purposes, but unfortunately all the benefits provided by such an instrument are quite expensive, meaning it is not always viable to have access to such quality instruments which can, in turn, affect the quality of one's findings.

There are also spectroscopy techniques such as Nuclear Magnetic Resonance (NMR) spectroscopy, Raman spectroscopy and fluorescence spectroscopy which all come with their fair share of benefits and shortcomings.

NMR spectroscopy is very good at identifying one-dimensional and two-dimensional spectra (Elipe, 2003; Santos *et al.*, 2017). This technique is also known for its easy sample preparation which allows for high reproducibility and quick results. The disadvantages of this technique are that it only picks up the required data if it possesses specific molecular isotopes (Santos *et al.*, 2017). Also, although the cost of analysing samples is low, the cost of obtaining the actual device is very high.

Raman spectroscopy is another spectroscopy technique that thrives on being able to detect high signal-to-noise ratios and reduce scattering in the data (Jehlička *et al*., 2003; Santos *et al*., 2017). However, its major drawback is its low sensitivity which is caused by the low probability of the Raman scattering event (Santos *et al*., 2017). This method also suffers from local thermal decomposition of samples especially when observed using UV or visible wavelength lasers (Jehlička *et al*., 2003; Santos *et al*., 2017).

Like the NMR technique, the molecular fluorescence technique also only requires a small number of samples and like the Raman technique, the molecular fluorescence technique has high signal-to-noise ratio, but what sets the molecular fluorescence technique apart from the previously mentioned techniques is its high sensitivity and specificity when it comes to spectral data analysis (Dumke and Teschner, 1988; Santos *et al*., 2017). However, this added advantage makes the sample preparation process for the molecular fluorescence technique fairly complex which can be seen as a major drawback for time sensitive projects (Santos *et al*., 2017).

2.5 Classification of multispectral imagery

Image classification serves a specific goal which is to convert image data into thematic data (Tempfli *et al*., 2009); this is because, in the application context, the interest lies in the thematic characteristics of an area (pixel) rather than in its reflection values. Thematic characteristics such as land cover, land use, soil type or mineral type can be used for further analysis and input into models. In addition, image classification can also be considered as a form of data reduction because the various multispectral bands result in a single band raster file (Tempfli *et al.*, 2009).

There are two types of classification approaches, namely: supervised classification and unsupervised classification (Tempfli *et al.*, 2009). In a supervised classification, the operator defines the clusters during the training process; while an unsupervised classification, on the other hand, refers to a classification in which a clustering algorithm automatically finds and defines a number of pixels with similar spectral features into one class (Tempfli *et al.*, 2009).

Supervised classification, as opposed to unsupervised classification, focuses on pre-defined classes (Tempfli *et al.*, 2009). The classifier can be built with a training set and later be used for classifying new objects. Supervised classification requires ground truth data, for labelling the classes, needed for training (Tempfli *et al*., 2009). Unsupervised classification clusters the data without prior definition of the groups (Tempfli *et al.*, 2009). This study only focused on supervised classification using ENVI and SNAP software.

Chapter 3: Materials and Methods

3.1 Introduction

This chapter describes the study area and outlines the materials and methods employed to acquire and process the rock samples as well as the remotely sensed images used in this study. Some of the methods used were derived from the research studies discussed in the literature review in Chapter 2.

3.2 Study Area

The Vredefort Dome (Figure 3) also known as the Vredefort impact structure is located 100 km southwest of Johannesburg in the South African province of Free State at latitudes and longitudes -27°00'0.00"S 27°29'59.99"E respectively (Gibson and Reimold, 2008). The Vredefort Dome, as named after the town located near its center was formed two billion years ago and its diameter was originally 380 km across making it the largest impact site but only the second oldest known impact crater on Earth (300 million years younger than the Suavjärvi Crater in Russia) (Gibson and Reimold, 2008; Ivanov, 2008; Simpson *et al.*, 2012).

Before 1937 when John Boon and Claude Albritton Boon provided evidence that the structure was caused by a meteorite, most people believed it was caused by a volcanic eruption (Bourgeois and Koppes, 1998; Marvin, 1999). Evidence of the meteorite impact site can be seen in the columns of granite that were injected into the existing rock by the force and heat of impact (Gibson and Reimold, 2008).

Due to its geological history and unique traits that attract a lot of tourists, the dome was inscribed as a World Heritage Site by UNESCO in 2005 and furthermore, there are plans to turn it into a research facility (Gibson and Reimold, 2008; Simpson *et al.*, 2012).

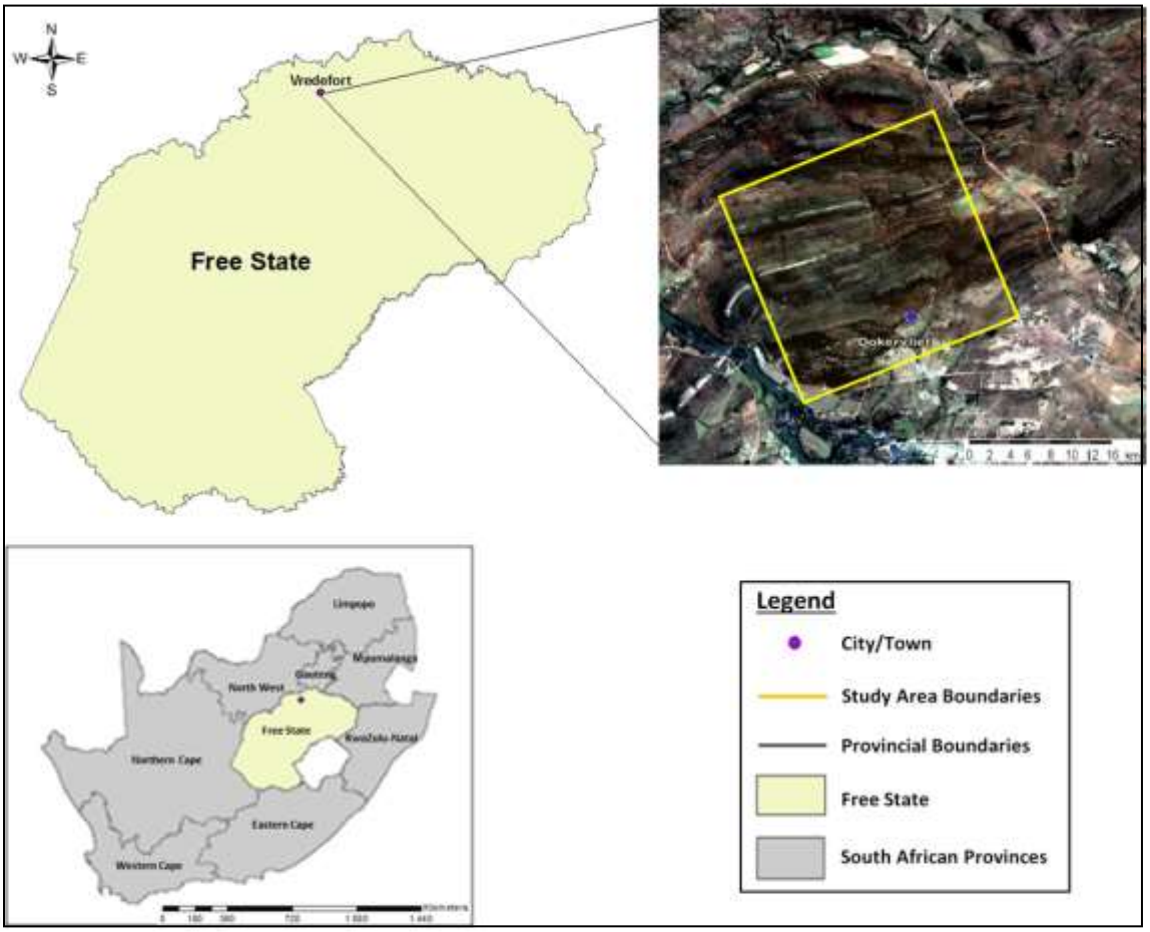

Figure 3: Location of Study Area

3.2.1 Climate and Rainfall

Using the Köppen-Geiger climate classification, climate in the Vredefort can be categorized as Cwb, i.e. there is much less rainfall in winter than in summer (Conradie, 2006; Kottek *et al.,* 2006). The average annual rainfall for Vredefort is 640.8 mm, with the area receiving the least precipitation (7 mm) in July and the most (111 mm) in January (Conradie, 2006; Climate-Data.org, 2012).

The normal midday temperatures for the area range from approximately 25.9°C in January to only 8.9°C in July (Conradie, 2006; Climate-Data.org, 2012). The rock samples utilized in this study were collected over a two day period (25^{th} and 26^{th} June 2018) and during this period the maximum daily temperature experienced during the day was never more than 24°C (AccuWeather.com, 2018). During the winter nights, temperatures have been known to drop to as low as -10°C, but during the data collection period temperatures only dropped to about -1°C (AccuWeather.com, 2018).

3.2.2 Layout of Region

The Vredefort Dome has a roughly semi-circular pattern of concentric ridges and plains of quartzite that can be recognized on topographic maps and satellite images especially towards the north-western portion of the dome (Bredenkamp and Van Rooyen, 1996; Conradie, 2006; Gibson and Reimold, 2008; Grieve *et al.*, 2008). The south-eastern portion of the dome, on the other hand, is not visible because it has been covered by sediments of the Karoo Supergroup and rocky highveld grassland vegetation (Bredenkamp and Van Rooyen, 1996; Lana *et al.*, 2003; Gibson and Reimold, 2008).

The Vredefort Dome is truncated by a series of valleys as well as the Vaal River which can be seen meandering the northern parts of the structure alongside the small town of Parys (Stepto, 1979; Conradie, 2006; Walt *et al.*, 2010). The short meandering streams are the ones that have given rise to the gullies and the valleys that cut through the hills of the dome (Stepto, 1979).

Due to the shallow and rocky soil type that can be found in the area, not a lot of agricultural activities take place in the Vredefort region except along the Vaal River and on the flatter surfaces in the surrounding areas (Bredenkamp and Van Rooyen, 1996). Livestock farming, on the other hand, is more prevalent in the area, although, due to the limited vegetation available to the animals for grazing, most farmers need to supplement the low nutrient content of the rocky highveld grassland vegetation with additional sources of nutrients as required by their livestock (Bredenkamp and Van Rooyen, 1996). Also, the steep slopes and unconsolidated rock debris present in the region can make it quite difficult for certain livestock to graze.

3.2.3 Geology

A core of basement granite marks the center of the Vredefort Crater (Gibson and Reimold, 2008; Reimold and Gibson, 2010). This core is surrounded by inclined rock units that dip away from the granite core in all directions to form a structural dome (Wieland *et al.,* 2005; Gibson and Reimold, 2008; Reimold and Gibson, 2010). It was created by a massive meteorite impact about two billion years ago that is about ten cubic kilometers in volume (Therriault *et al.,* 1997; Gibson and Reimold, 2008). It displays a volcano-metasedimentary sequence of rocks as well as igneous intrusions and one extrusion (Gibson and Reimold, 2008; Reimold and Gibson, 2010).

The rocks in the volcano-metasedimentary sequence are quartzite, metapelite, meta-ironstone, banded ironstone and olistostrome (Gibson and Reimold, 2008). The intrusions, which cross-cut the volcano-metasedimentary sequence, are made up of granite, dolerite as well as impact-melt rock (Gibson and Reimold, 2008). The extrusion present is of basalt origin (Gibson and Reimold, 2008).

Due to changes in temperature and pressure, the rocks in this area have undergone modifications (metamorphism). The evidence of this is shown by the existence of metamorphic features such as the impact-melt rock (Reimold and Gibson, 2010). The rocks in this area were metamorphosed at metamorphic facies such as the granulite to greenschist to amphibolite facies (Flowers *et al.,* 2003; Reimold and Gibson, 2010). As a result of a strong increase in temperature leading to the metamorphism, the rocks do not display their original textures, and mineralogy well (Gibson and Reimold, 2008; Reimold and Gibson, 2010).

There are three types of metamorphism, namely, regional, contact and shock metamorphism. Regional metamorphism as the name suggests is a type of metamorphism where the minerals and texture of a rock are manipulated by heat and pressure that can occur over a wide area or region (Stepto, 1979). Contact metamorphism, on the other hand, occurs around intrusive rocks as a result of an increase in temperature that is caused by the intrusion of magma (Stepto, 1979). Lastly, what sets apart shock metamorphism from the previously mentioned types of metamorphism is that it occurs when a meteorite collides with the earth’s surface during an extremely violent volcanic eruption (Reimold and Gibson, 2010).

Stepto (1990) suggested that the modification of the rocks in the Vredefort Dome was a result of shock metamorphism during the formation of the Dome. He suggested that this event led to the development of abundant pseudotachylites and a brittle cleavage present in most rocks in the region. However, more recent literature has suggested that the rocks of the Vredefort Dome actually display textural evidence of a two-stage metamorphic history (Stepto, 2005; Lieger *et al.,* 2009; Reimold *et al.,* 2017).

The Vredefort granulites are said to have undergone unusually rapid and highly variable heating, exhumation and cooling, while other rocks have been metamorphosed at metamorphic facies (Flowers *et al.,* 2003). The main source of heat here is the meteorite impact itself because the igneous intrusions themselves have been metamorphosed (Flowers *et al.,* 2003). Also, some rocks in the Dome underwent a unique type of metamorphism known as cataclastic metamorphism which occurs when rocks get grinded and pulverized as they shifted along an active fault (Miyashiro, 2012). This led to these aforementioned rock types having a unique texture that differentiates them from the rest of the metamorphosed rock types that appear in the Dome.

3.2.3.1 Physical and Chemical Properties of Rocks from the Vredefort Dome

As aforementioned, the majority of rocks in the Vredefort region have undergone metamorphism due to the impact; and more specifically in the Donkervleit area, these rocks all seem to have a similar orientation in which they all dip in the south-west direction.

The oldest rocks are exposed to the south, while the youngest rocks seem are found in the north of the Donkervleit area (Gibson and Reimold, 2008). What this essentially means is that this sequence of rocks follows the laws/principles of superposition which state that rocks get younger as we move up the stratigraphic column.

Also, the sequence of these rocks can be referred to as conformable because there is no evidence of extensive erosion that would have led to a period of non-deposition. However, at the base of the sequence, there is a contact between granite which can be referred to as a type of nonconformity. Throughout this research these rock types will be described in their stratigraphic order as related to their supergroups (Figure 4), from oldest to youngest, namely: granite gneiss, basalt, quartzite, meta-ironstone, banded iron formation, metadolerite and metapelite.

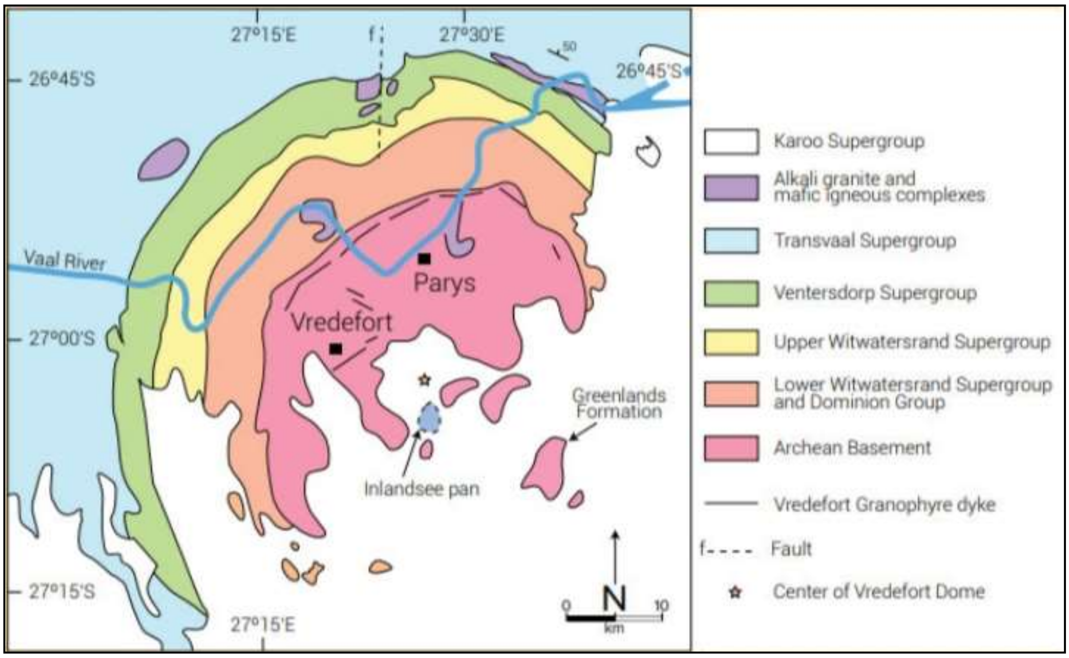

Figure 4: Geological Map of the Different Supergroups in the Vredefort Dome (Reimold and Koeberl, 2014)

3.3 Data and Methods

3.3.1 Field and Lab Data Acquisition, Description and Processing

In the field, rock samples of quartzite, meta-ironstone, banded iron formation (BIF), basalt, meta-dolerite, meta-pelite and granite were collected through a widely used geological sampling technique which involves making knowledgeable observations in linear transects, which in this study refer to the lower, middle and upper regions of the dome in the Donkervleit area (Debba *et al.,* 2005). The convenience sampling approach which is a non-probability sampling method (Congalton and Green, 2008) was also adopted due to the steep terrain in some of the locations of the study area which made it difficult to collect the necessary rock samples.

Along this transect, the locations of each of the collected rock samples were also recorded using a GPS (Table 3). It should be noted though, that under normal conditions the spectral signatures of these rocks would have been captured *in situ* but due to not having the spectroradiometer readily available, the rocks had to be broken off from the parent rock, carefully placed in clearly marked plastic bags and brought back to the lab where they were placed in an environment that mimicked the natural climatic conditions of the study area (as mentioned in section 3.2.1) in order to obtain the spectral signatures required to carry out this study (Figure 5) (Bertel *et al*., 2006; Anbazhagan and Arivazhagan, 2010).

Once the temperature conditions were similar to the ones experienced during the collection of the samples (section 3.2.1), the first step was to calibrate the Spectral Evolution spectroradiometer using a spectralon white reference panel and only then could the target measurements be collected (McCoy, 2005). The Spectral Evolution SR-3500 is a spectroradiometer that measures spectra between 0.35 µm and 2.5 µm and has a bandwidth of 0.001 µm (spectralevolution.com, 2004). It is fitted with lenses of varying angles to allow to measure a variety of objects and it even comes with a contact probe that contains its own light source which aids in the process of obtaining spectral radiance measurement of the collected samples (spectralevolution.com, 2004).

In order to obtain the best results, guidelines from McCoy (2005) were followed and the contact probe was held at a zenith angle of 0^{o} at a distance of no more than 10 mm directly above each collected rock sample, so as to avoid casting shadows that could distort the results. The background noise which is created by energy from thermal fluctuations is always present, but it can be dealt with by introducing a dark spectrum. The Spectral Evolution SR-3500 comes standard with an automatic dark mode option which was used to remove the background noise.

A minimum of three measurements were taken in various parts of each rock sample and saved with an explicit name in the device's directory (McCoy, 2005). This was done so that each averaged sample can be used as representatives of the rock modal composition (Sgavetti *et al.*, 2006). These steps were repeated until the NIR-IR spectra of each rock type was collected.

The Spectral Evolution SR-3500 also comes with PC software that enables you to display and extract the data collected by the device (spectralevolution.com, 2004). Therefore, once all the measurements were collected, the spectroradiometer was connected to a PC using a USB cable and all the relevant measurements were selected and transferred to an excel spreadsheet which was used to upload this data into the ENVI software for further remote sensing analysis.

The next step that followed was the upscaling of the data to get it to the same resolution as the Sentinel-2 image data. This was done so that the data could be used as references for the spectral matching and lithological classification process. Within the ENVI software, the relevant tab options were selected in order to average the target measurements collected for each rock type and plot their reflectance curves. The continuum removal technique was then employed to help normalize the reflectance spectra. This normalized data was used as the input parameters under the analyst tools tab option offered by ENVI in order to generate the spectral library required for this study.

Until this point, the rock samples were required in their most solid and natural state, but once the collection of the spectral signatures was done, the rock samples were then sent through to the Geosciences laboratory where small portions of these samples were broken down and grinded into a homogeneous powder using crushing and milling equipment and sent through to experts for XRF analysis which could accurately depict the chemical composition of each rock type in order to determine the unique and overlapping mineral contents of these rocks (Figures 6 and 7).

Table 3: GPS Coordinates of Where Each Rock Type Was Located

Name	**Coordinates**	**Elevation (m)**
Granite Gneiss	26°52’48.85“S 27°23’04.45“E, 26°52’47.67“S 27°23’02.38“E 26°52’53.81“S 27°23’08.48“E, 26°52’53.77“S 27°23’08.38“E	1400 1401 1402 1407
Basalt	26°52’51.63“S 27°23’02.38“E, 26°52’51.67“S 27°23’02.18“E, 26°52’51.46“S 27°23’01.71“E, 26°52’27.01“S 27°23’05.05“E	1418 1418 1420 1458
Quartzite	26°52’18.77“S 27°23’07.34“E, 26°52’18.61“S 27°23’07.48“E, 26°52’16.45“S 27°23’03.72“E, 26°52’14.00“S 27°23’08.13“E	1510 1511 1513 1517
Meta-Ironstone	26°52’14.23“S 27°23’08.18“E, 26°52’13.35“S 27°23’07.83“E, 26°52’13.29“S 27°23’07.94“E, 26°52’12.77“S 27°23’07.34“E	1518 1512 1512 1505
Banded Iron Formation	26°52’12.83“S 27°23’07.46“E, 26°52’09.93“S 27°22’57.80“E, 26°52’09.24“S 27°22’57.59“E, 26°52’08.87“S 27°22’45.51“E	1506 1426 1420 1445
Metadolerite	26°52’07.78“S 27°22’45.14“E, 26°52’07.58“S 27°22’45.10“E, 26°52’05.48“S 27°22’45.66“E, 26°52’05.48“S 27°22’45.53“E	1451 1452 1457 1458
Metapelite	26°52’05.76“S 27°22’42.06“E, 26°52’05.37“S 27°22’41.03“E, 26°52’05.38“S 27°22’40.77“E, 26°52’05.42“S 27°23’40.84“E	1475 1483 1484 1486

Figure 5: Spectral Evolution Spectroradiometer Being Prepared to Use for Spectral Signature Collection

Figure 6: Crushing and Milling Equipment in the Geosciences Lab

Figure 7: Crushed Rock Samples Ready for XRF Analysis

3.3.2 Satellite Data Acquisition, Description and Preparation

The identification of surface materials on satellite imagery is best achieved by deriving the spectral reflectance of the materials (Tempfli *et al.*, 2009). That is particularly the case when satellite imagery analysis is supported by ground-collected spectral libraries (Song *et al.*, 2001; Hadjimitsis and Clayton, 2008).

Radiance is best described as the amount of radiation coming from an area and it accounts for the effects of absorption and scattering of the atmosphere (Xu and Huang, 2008; Gao *et al*., 2009; Tempfli *et al*., 2009). Reflectance, on the other hand, refers to the proportion of the radiation striking a surface and reflecting off of it (Tempfli *et al*., 2009). This means that, in order to identify certain materials, such as the surface geology of a particular region, the surface reflectance from an image's data needs to be derived, and this can only be achieved once atmospheric corrections are carried out.

A Sentinel-2 sub-scene (S2A_MSIL2A_20170405T075611_N0204_R035_T35JNL) of the Vredefort Dome area was acquired a week after its release (12^{th} of April 2017), from the ESA's Copernicus Programme portal (https://scihub.copernicus.eu/dhus/#/home). For visualization and interpretation purposes, this image was then atmospherically corrected and rectified to a common UTM coordinate system (UTM WSG 84 35S). The Sentinel-2 20 m resolution data used was resampled to correspond to the VNIR 10 m spatial dimensions using an algorithm in the SNAP software which enabled the image to keep its original pixel brightness values. Then the band ratioing technique was utilized so as to enhance the spectral differences between bands and also reduce the shadow effects caused by the topography of the Donkervleit region. Geometric corrections were not conducted for this study because geometric corrections normally deal with terrain relief and they can be neglected when using the 2-dimensional approach which is the approach used in this study (Tempfli *et al*., 2009).

Once the images were processed and atmospherically corrected, it became a priority to identify the spectral ranges and bands required for a geological study such as this. Since the rocks in the Vredefort Dome have undergone metamorphism, the bands selected had to be in compliance with the ranges suitable with these types of rocks. It was found that the most suitable bands from the Sentinal-2 images obtained, were bands 3, 4, 8, 11 and 12 (Kruse, 2012; Ge *et al.*, 2018).

The next step was masking the vegetation present in the images in order to prevent the vegetation reflectance from interfering with the main purpose which was to extract geological information. This was done using the mask manager tool in SNAP which calculated the NDVI, where R_x was assumed to be the reflectance value at a red (Red) or near-infrared (NIR) wavelength in the VNIR range. Thereafter, basic image processing skills such as producing colour composites with saturation stretch and classification had to be applied so as to extract the relevant geological information required for this study.

3.4 Geological Mapping

As previously mentioned in the literature review, different methods exist to map mineral occurrences included in a spectral library. For this study, the Spectral Angle Mapper (SAM) approach was used mainly because of its lithological discrimination capabilities as well as its ability to minimize the albedo effect while still remaining sensitive to the absolute values of the spectral features being studied. (Ge *et al.*, 2018).

3.4.1 Spectral Angle Mapper

Spectral matching is a pre-classification process in which spectral profiles of selected pixels of targets are compared with the library profiles (Kruse and Perry, 2009; Tempfli *et al*., 2009; Amrutkar *et al*., 2016). There are two main types of spectral matching namely: manual matching and automated matching. For this study, the Spectral Angle Mapper (SAM) automated matching option was chosen and used within the ENVI software. This technique is, in fact, a pixel-based classification which was used to measure the similarities of each pixel signature with the spectra curves in the spectral library. SAM stood out as the best technique to use for this study due to the fact that it is not affected by direct sunlight or shadow effects that can be caused by the varying topography found in the study area.

3.5 Accuracy Assessment

Data analysis refers to how the raw data has been selected, combined and evaluated. In this study, the analysis process included validation of results in order to assess the accuracy of the classification outcomes. Most of the results were calculated using ENVI, SNAP and R-Studio software. Thereafter they were placed into Microsoft Excel spreadsheets that were utilized for analysis purposes in the results and discussion section.

For the purposes of this study, an accuracy assessment was conducted using the post-classification method on ENVI Classic software. From this, a confusion matrix was produced in order to validate the results by comparing the classified image to the geological map generated by fieldwork.

The accuracy for each class was determined by taking the number of correctly identified pixels within the displayed area and dividing that number by the sum of all the numbers combined (within those respective rows or columns) including error pixels of commission and omission (Congalton, 1991; Congalton and Green, 2008). This method tends to produce an accuracy that is lower than that of the overall classification (Tempfli *et al*., 2009).

Overall accuracy is the number of correctly classified pixels (i.e., the sum of the diagonal cells in the error matrix) divided by the total number of pixels checked (Tempfli *et al.*, 2009). It should be noted that 'reference data' can refer either to data derived from field observations or from sources of an assumed higher accuracy such as aerial photos and pre-existing field checked maps (Tempfli *et al.*, 2009). In this study, the former rather than the latter approach was used because field work needed to be conducted in order to collect the rock samples needed for the spectral signature analysis.

For each rock type, 50 points were collected (35 training sites and 15 test sites) and these points were used to create a confusion error matrix which was used to validate the results by comparing the classified image to the geological map created from the field observations. The overall accuracy, user accuracy, and producer accuracy were calculated for the Sentinel-2 classified map.

3.6 Summary of Methods

The flowchart below (Figure 8) summarizes all the processes used in the materials and methods section.

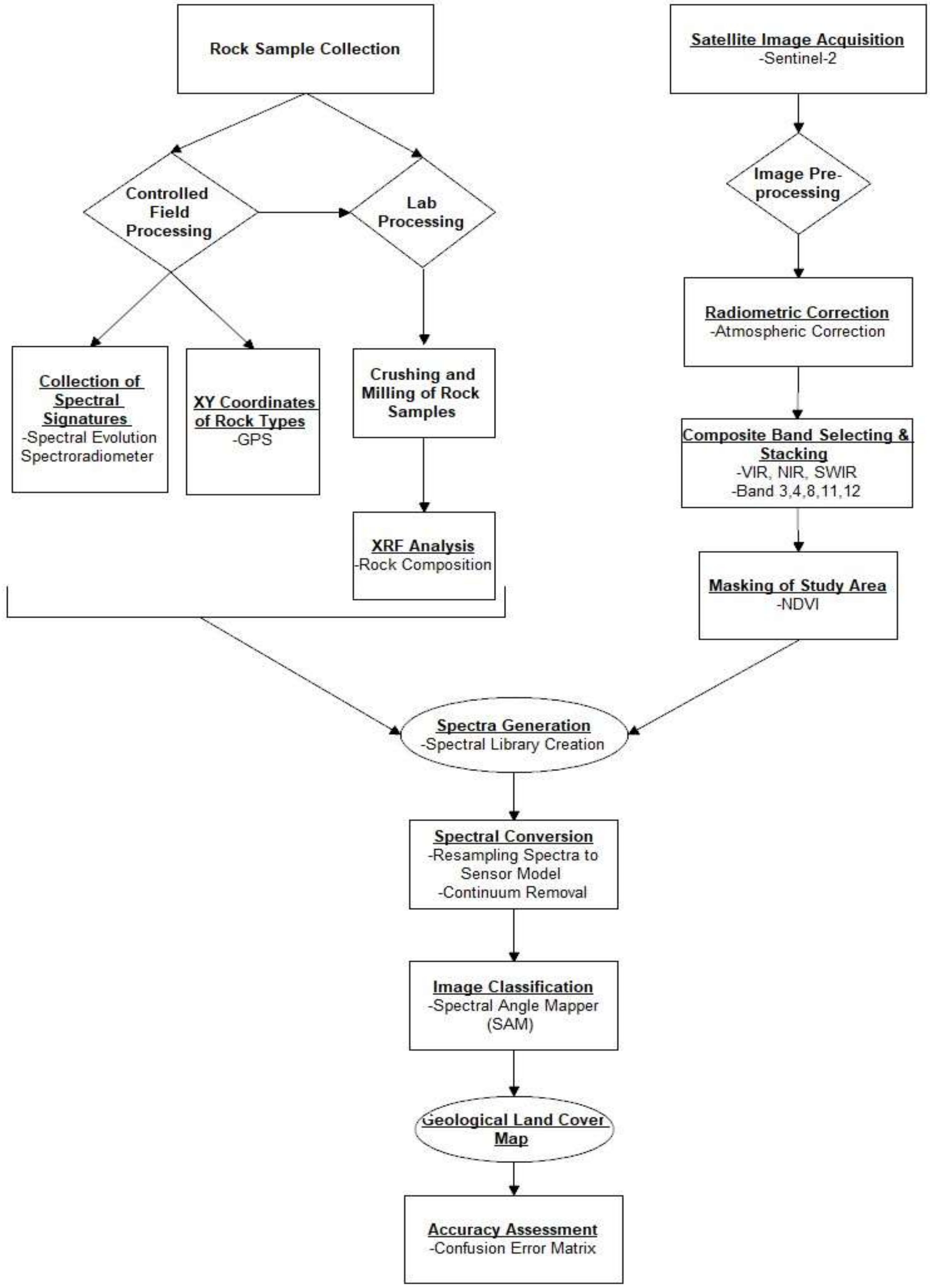

Figure 8: Methods and Material Summary Flow Chart

Chapter 4: Results

4.1 Introduction

This chapter presents the results as per the aims and objectives of this study, followed by a brief discussion which will be linked to the literature where applicable. The results include: the normalized spectral reflectance of each rock type using the continuum removal method as well as the spectral library created from the assessed spectral signatures. Lastly, a map showing the spatial distribution of the rocks present in the study area as well as an accuracy assessment matrix of the classification results are included.

4.2 Spectral Reflectance of Samples

The spectral reflectance of most rock types can be observed in the VNIR (visible and near infrared) and SWIR (shortwave infrared) region of the spectrum (0.4 µm – 2.5 µm). It is in this region that useful information can be obtained on the diagnostic absorption features of each rock type (Crowley *et al.*, 2003). This is mainly because of the presence of OH and other hydroxyl bonds such as Mg-OH and Al-OH in the aforementioned regions of the spectrum (Crowley *et al.*, 2003; Qaid and Basavarajappa, 2008).

Reported below are the results from the samples collected from the controlled field site using the Spectral Evolution spectroradiometer. As can be seen from the spectral reflectance graphs of each sample, three measurements were taken from each sample, averaged and then used as representatives of the rock modal composition (Sgavetti *et al*, 2006). In addition, in order to accurately determine the diagnostic absorption features of each rock sample, the continuum removal method was applied.

4.2.1 Granite Gneiss

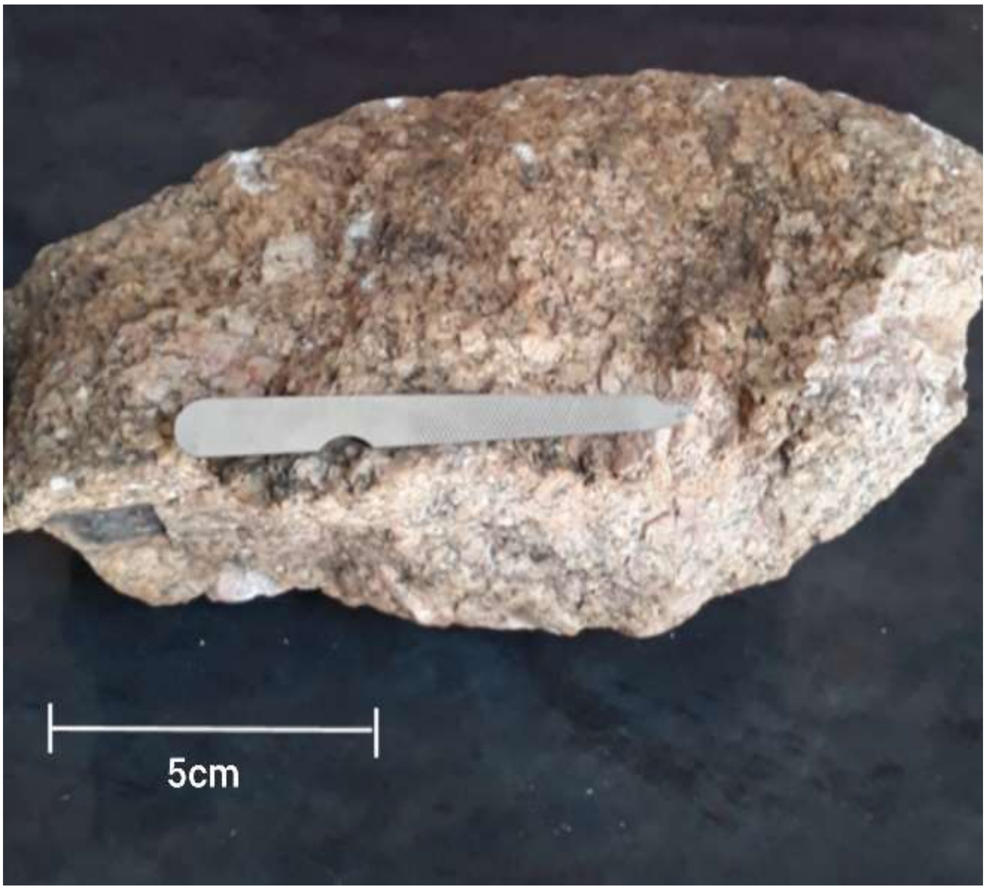

Figure 9: Granite Gneiss Rock Sample Collected from the Study Area

Granite is an igneous rock and before it undergoes metamorphism it is referred to as having a phaneritic texture (Nesse, 2009). In the Vredefort region, the granite gneiss is the basement rock and it acts as an intrusion, meaning it does not officially form part of the main stratigraphic succession or column (Gibson and Reimold, 2008). The granite gneiss rock samples observed in the study area were brown to pinkish in colour and had a grain size that varied from medium (1 mm across) to coarse (10 mm across) per individual crystal (Figure 9).

This heterogeneous rock type contains the following minerals with an approximate estimate of their abundances: K-Feldspar: 60%, Quartz: 20%, Plagioclase: 20% (Nesse, 2009).

(a)

(b)

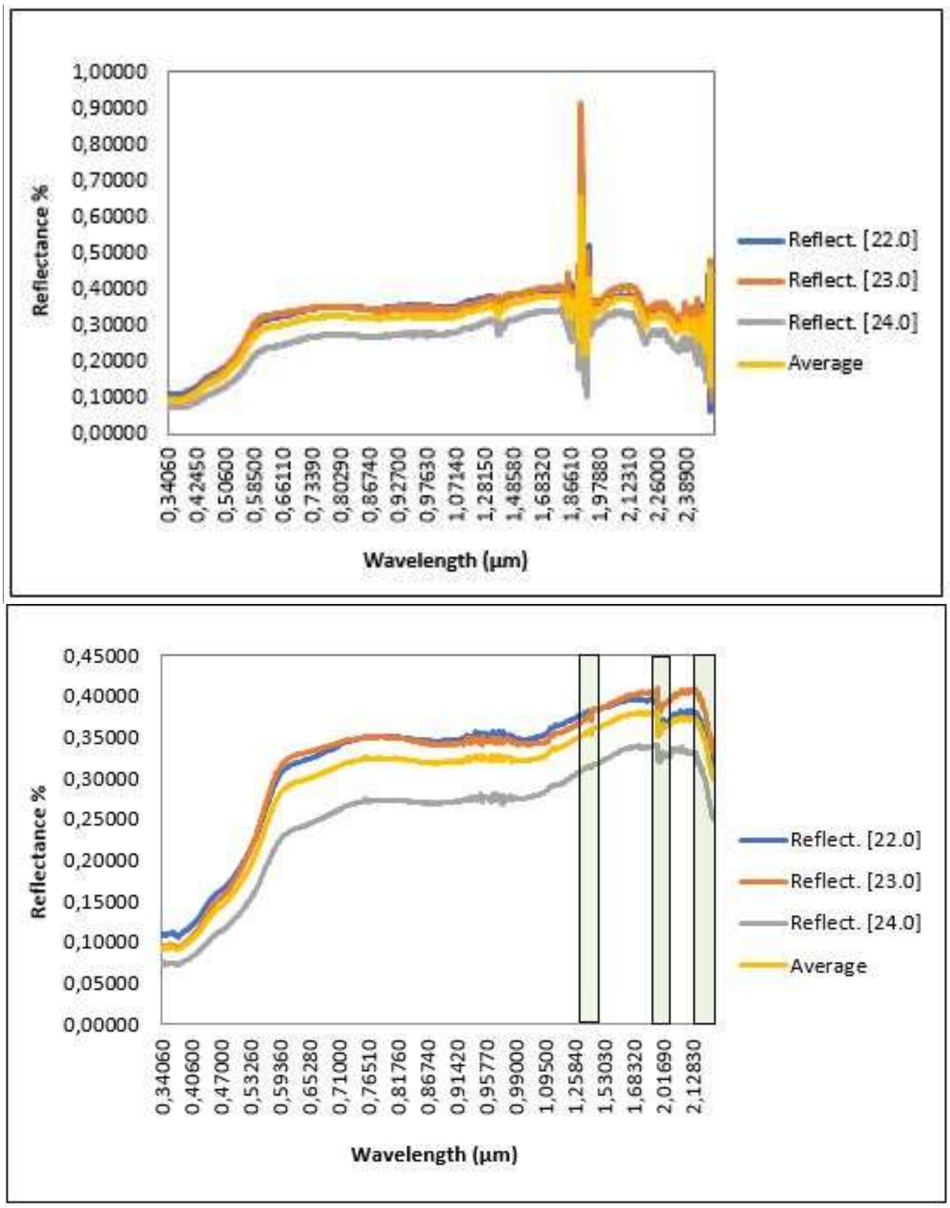

Figure 10: Reflectance Spectra of Granite Gneiss: (a) Before Continuum Removal, (b) After Continuum Removal

Metamorphic rocks such as gneisses are formed by the metamorphism of schists under high-grade conditions and they usually consist of mineral components that are not noticeable in the VIR (Visible-Near Infrared) region (Longhi *et al*., 2001; Nesse, 2009). However, granite gneiss does consist of plagioclase which presents absorption features around 1.35 µm; muscovite at 2.00 µm; followed by a relatively weak quartz absorption trough at 2.14 µm and ending off with absorption features, which can be attributed to the presence of biotite, at 2.20 µm. Apart from this, the spectrum is fairly smooth in nature (Figure 10b).

4.2.2 Basalt

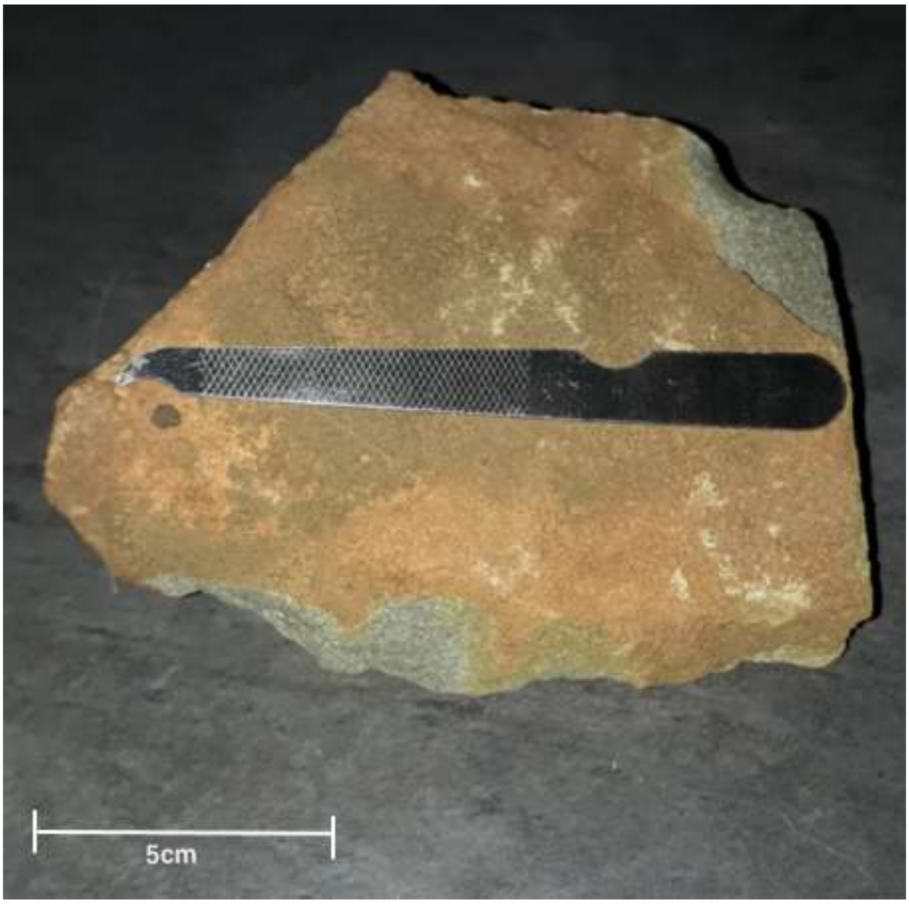

Figure 11: Basalt Rock Sample Collected from the Study Area

Basalt is a mafic extrusive igneous rock formed from the rapid cooling of magnesium-rich and iron-rich lava exposed at or very near the surface of the Earth (Reimold and Gibson, 2010). The basaltic rocks present in the study area are fine-grained (<1 mm across), black to dark grey in colour and possess euhedral to subhedral plagioclase porphyroblasts which contribute to their porphyroblastic texture.

It contains the following minerals with an approximate estimate of their abundances:
Pyroxene: 65%, Plagioclase: 20%, Olivine: 15% (Nesse, 2009).

(a)

(b)

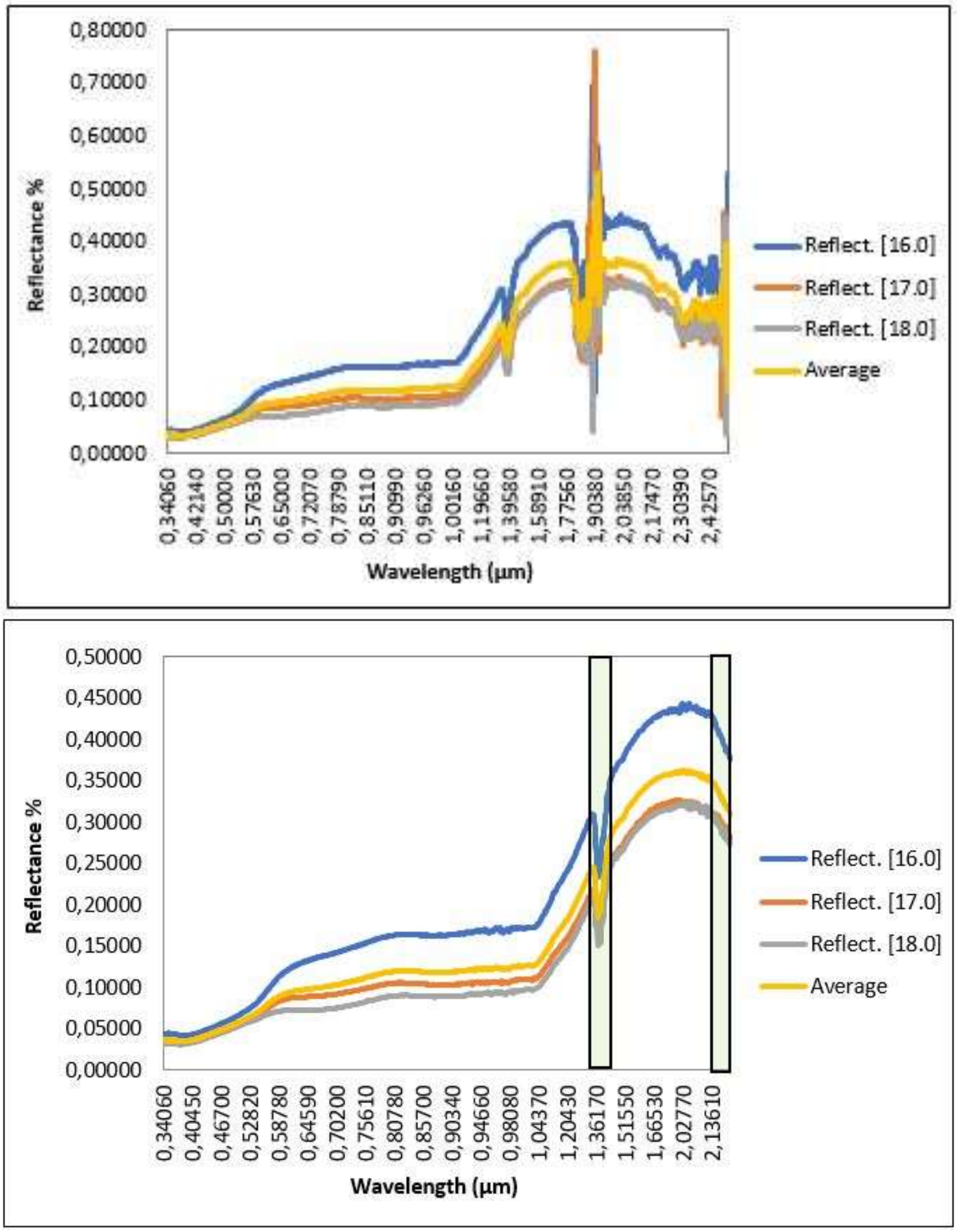

Figure 12: Reflectance Spectra of Basalt: (a) Before Continuum Removal, (b) After Continuum Removal

Within the range of 0.4 to 2.2 µm, there is variability in the spectral reflectance of basalt across the spectrum. One of the noticeable features is a reflectance peak at 1.33 µm which is in the SWIR region. This is closely followed by an absorption trough at 1.36 µm and there also seems to be another absorption trough that takes place at 2.20 µm which still represents the SWIR region of the spectrum.

4.2.3 Quartzite

Figure 13: Quartzite Rock Sample Collected from the Study Area

When quartz sandstones endure enormous amounts of heat and pressure, they convert into quartzite (Chen *et al.,* 2011). Quartzite rocks tend to be fine to medium grained (1-10 mm across) with sub-rounded mineral crystals that are visible to the naked eye. These white to cream coloured rocks usually consist of high levels of quartz (close to 85% in certain specimens), with smaller amounts of fuchsite and potassium feldspar as well as negligible traces of iron (Fe) (Nesse, 2009).

Most of the quartzites found in the Donkervleit area seemed to exhibit conchoidal fractures on their surfaces and there were some which exhibited a planar-cross bedding sedimentary texture which is indicative of overturned strata. There also seemed to be a slight difference in the mineral composition of the quartzite rocks found at the top of the ridge versus those found further down on the sides. It seems that the quartzites at the top of the ridge are oversaturated with quartz (up to 90%) whereas the ones found further south of the ridge seemed to become enriched with fuchsite which gave them their greenish colour and potassium feldspar which gave others their pinkish colour.

(a)

(b)

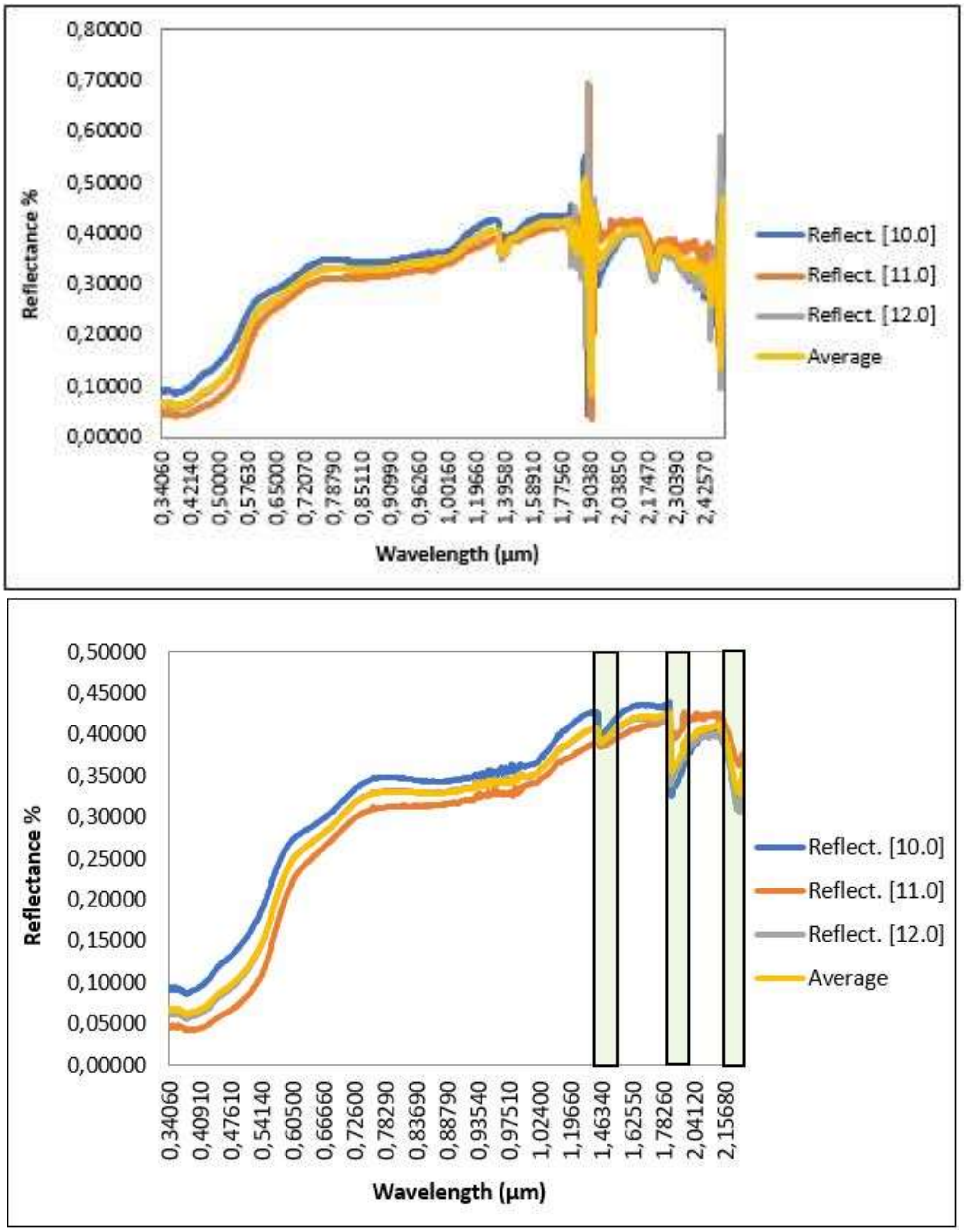

Figure 14: Reflectance Spectra of Quartzite: (a) Before Continuum Removal, (b) After Continuum Removal

As aforementioned, the main mineral components of gneisses are not usually detectable in the VIR region and neither are those of quartzites unless there are impurities present (Gupta, 2003). Quartzites consist of more than 90% of quartz and the ones present in the Vredefort Dome have a higher albedo than any other rocks present in the area. As can be seen from the reflectance spectra of quartzite in Figure 14b, there are clear absorption features at 1.45 µm, 1.95 µm and 2.20 µm.

4.2.4 Meta-Ironstone

Figure 15: Meta-Ironstone Rock Collected from the Study Area

Meta-ironstones are fine to medium grained rocks that usually originate from sandstones or limestones that contain more than 15% iron (Nesse, 2009). According to literature, most ironstones formed during a period when oxygen wasn't as abundant, in the atmosphere, as it is now and as such, we are seeing fewer and fewer occurrences of ironstones in the natural environment (Gibson and Reimold, 2008; Reimold and Gibson, 2010).

They often have an abundance of iron-bearing minerals such as hematite, magnetite, goethite, siderite, and chamosite which even after metamorphism contribute to the magnetic as well as the dark coloured characteristics that this rock type usually possesses (Gibson and Reimold, 2008; Reimold and Gibson, 2010). Most of the meta-ironstones in the study region are homogeneous, have compositional layering and are broken along parallel surfaces (i.e. have cleavage). Some of the rocks even exhibited a hummocky cross-stratification as their sedimentary structure (Gibson and Reimold, 2008).

(a)

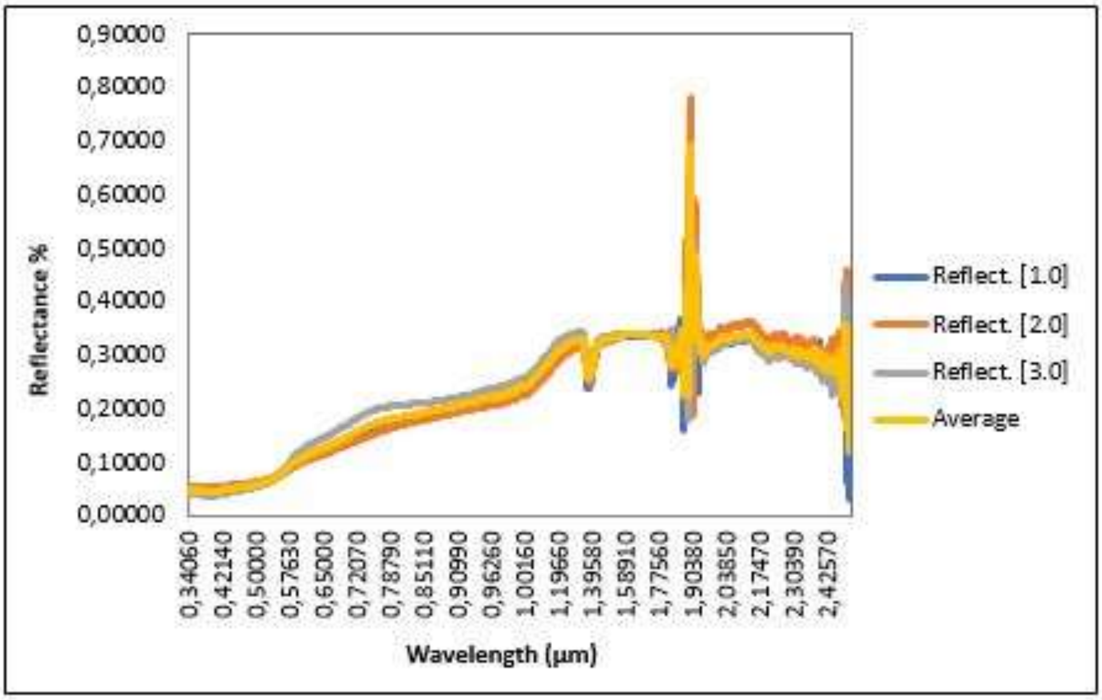

(b)

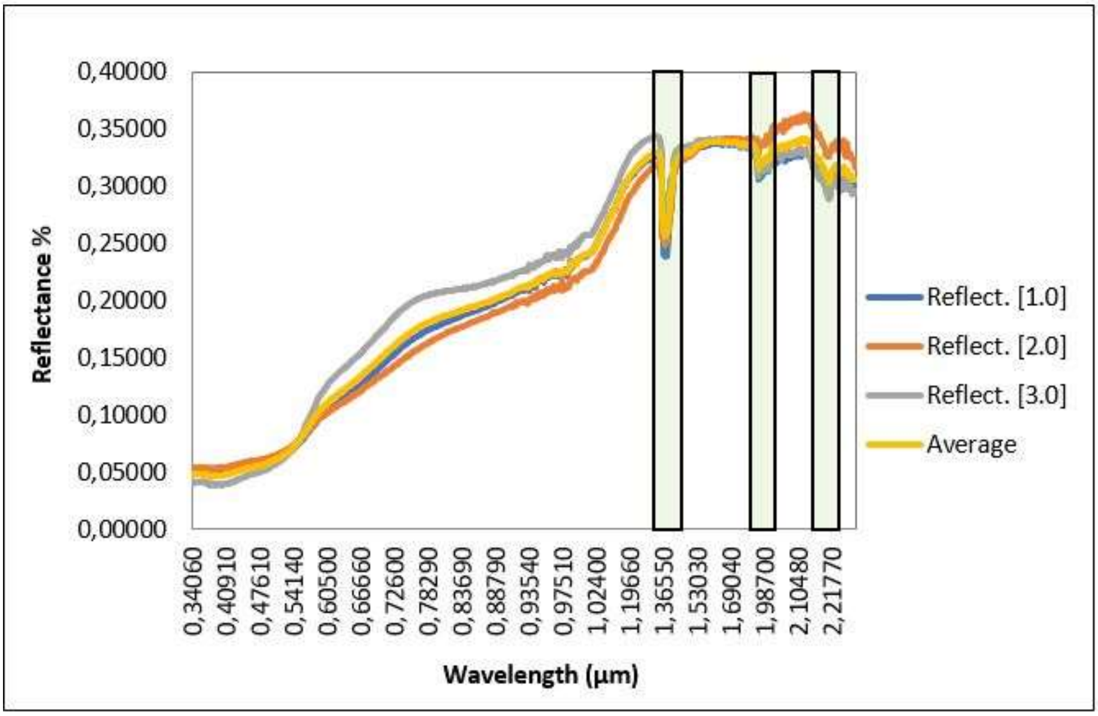

Figure 16: Reflectance Spectra of Meta-Ironstone: (a) Before Continuum Removal, (b) After Continuum Removal

Meta-ironstones tend to be iron-rich and this is why this sample's reflectance spectra shows a clear and strong absorption trough at 1.38 µm (Figure 16b). This is followed by three weak absorption features at 1.96 µm, 2.21 µm and 2.23 µm; all of which belong to the Short-Wave Infrared (SWIR) region of the spectrum.

4.2.5 Banded Iron Formation

Figure 17: Banded Iron Formation Rock Sample Collected from the Study Area

Banded ironstones, also known as banded iron formation (BIF) are usually fine to medium-grained rocks that date back to the Precambrian era (Gibson and Reimold, 2008). The banding exhibited by these rocks, is widely accepted to be as a result of cyclic variations in oxygen availability (Reimold and Gibson, 2010). They have the ability to form very thick sequences and in some parts of the world, such as in the Hammersley Range of Australia, they are well sought-after because of their ability to act as a profitable source of iron ore (Wårell, 2007).

The banded ironstones found in the study area are mainly brown in colour and consist of weathered bands which range from about 2 mm to 7 cm in thickness. These bands are created from alternating layers of magnetite (Fe_3O_4), hematite (Fe_2O_3), iron oxide (FeO) as well as iron-deficient shales and cherts which contribute to BIF's reddish colour (Gibson and Reimold, 2008; Nesse, 2009).

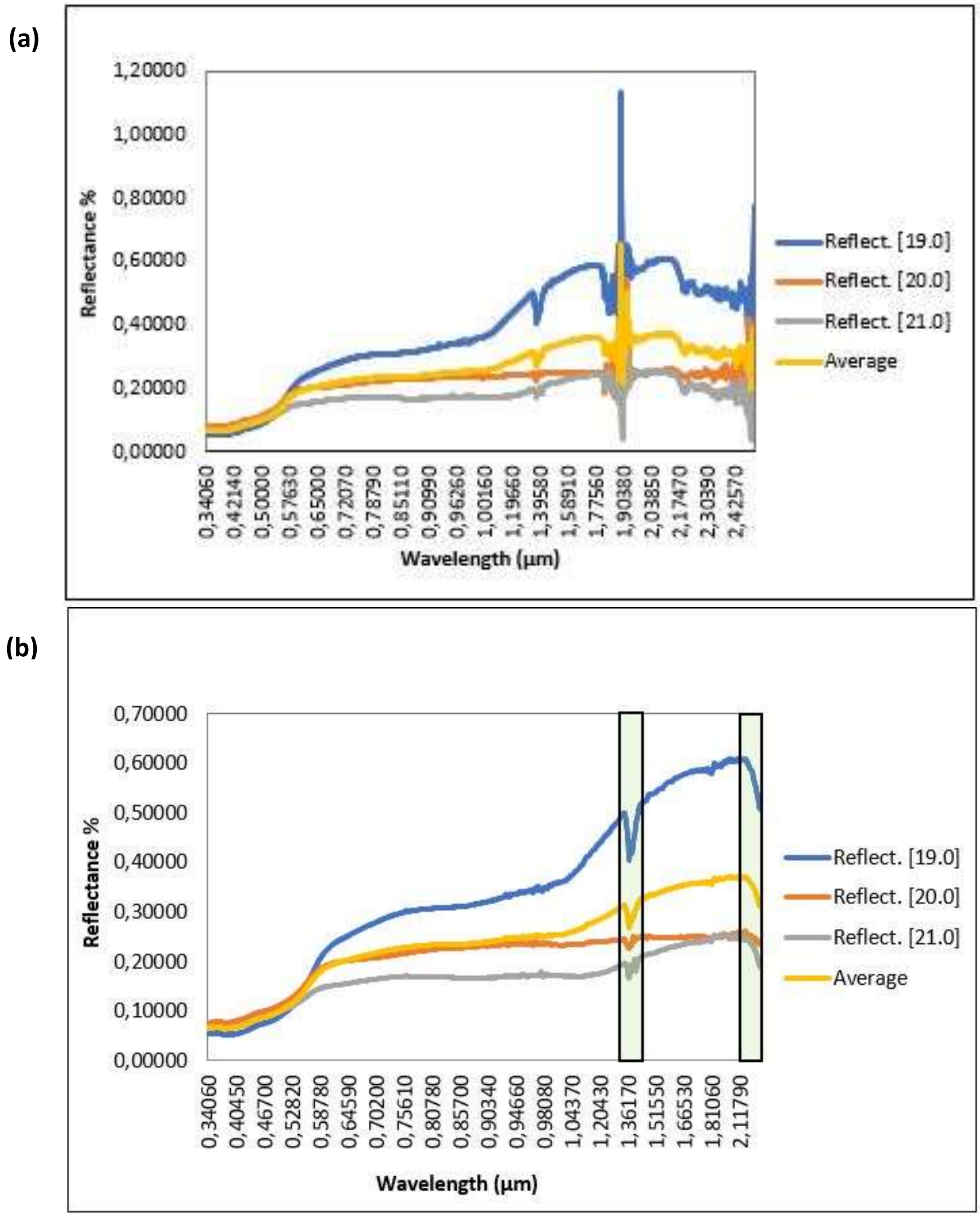

Figure 18: Reflectance Spectra of Banded Iron Formation: (a) Before Continuum Removal, (b) After Continuum Removal

Banded iron formations (BIF) are usually fine-grained, dark in colour and possess alternating layers of iron-rich oxides and silicate minerals, which give them their banded status (Gibson and Reimold, 2008). It is the presence of these iron-rich oxides that contribute to the absorption features that can be seen at 1.38 and 2.20 µm (Figure 18b).

4.2.6 Metadolerite

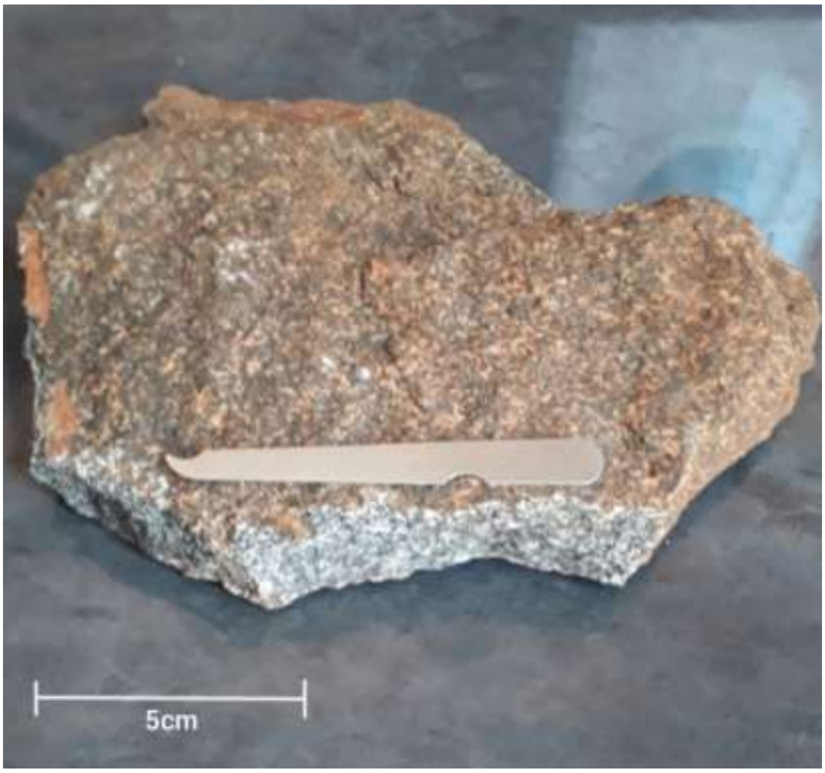

Figure 19: Metadolerite Rock Sample Collected from the Study Area

The metadolerite is very hard and magnetic, which is indicative of the mineral magnetite which forms the fine to medium-grained greyish matrix and makes up about 30% of the rock's mineral composition (Gibson and Reimold, 2008; Nesse, 2009). This rock type also consists of about 50% plagioclase crystals which are white in colour and angular in shape. The remaining 20% of the rock is usually made of pyroxene which also acts as a matrix mineral.

The metadolerites present in the Vredefort Dome act as intrusions and because of their fine-grained igneous origin possess an aphanitic texture (Gibson and Reimold, 2008). These heterogeneous rocks, which also exhibit ripple-like lamination, lay in horizontal beds which mean they do not have any specific orientation (Gibson and Reimold, 2008).

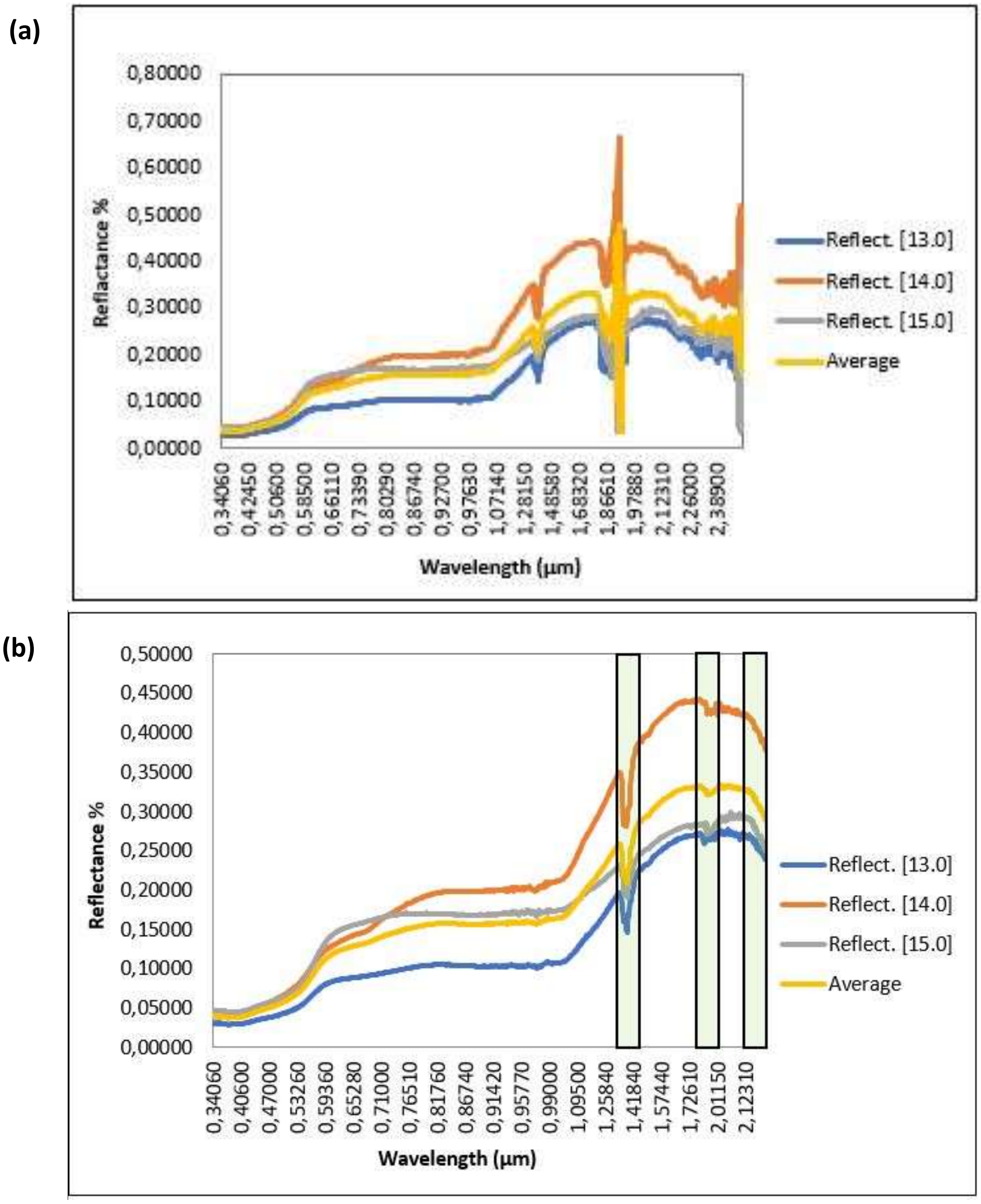

Figure 20: Reflectance Spectra of Metadolerite: (a) Before Continuum Removal, (b) After Continuum Removal

The Spectral Evolution results for the metadolerite samples collected exhibit absorption features at 1.38 µm due to the presence of minerals such as plagioclase and pyroxene. There also seems to be points of inflection at 1.97 µm, 2.04 µm, and 2.15 µm (Figure 20b) which may be attributed to the impurities caused by iron-bearing minerals.

4.2.7 Metapelite

Figure 21: Metapelite Rock Sample Collected from the Study Area

Metapelitic rocks are brownish to black in colour; with the brownish surfaces being present due to weathering. These rocks are derived from sedimentary pelitic rocks that have undergone contact or regional metamorphism and tend to be highly distinguished due to the fact that clays are very sensitive to temperature and pressure changes (Gibson and Reimold, 2008). They have compositional layering where individual mineral grains are aligned according to different compositions (Nesse, 2009).

The different minerals were changed as a result of metamorphism. The minerals they contain are potassium feldspar which is pinkish in colour, magnetite which is black in colour, cordierite which is greyish in colour and lastly andalusite crystals which are brownish in colour and are referred to as porphyroblasts thus giving this rock type its porphyroblastic texture (Gibson and Reimold, 2008). Chemically these rocks are rich in Al_2O_3 and SiO_2 and also have a significant amount of Na_2O and K_2O but are usually poor in CaO (Gibson and Reimold, 2008).

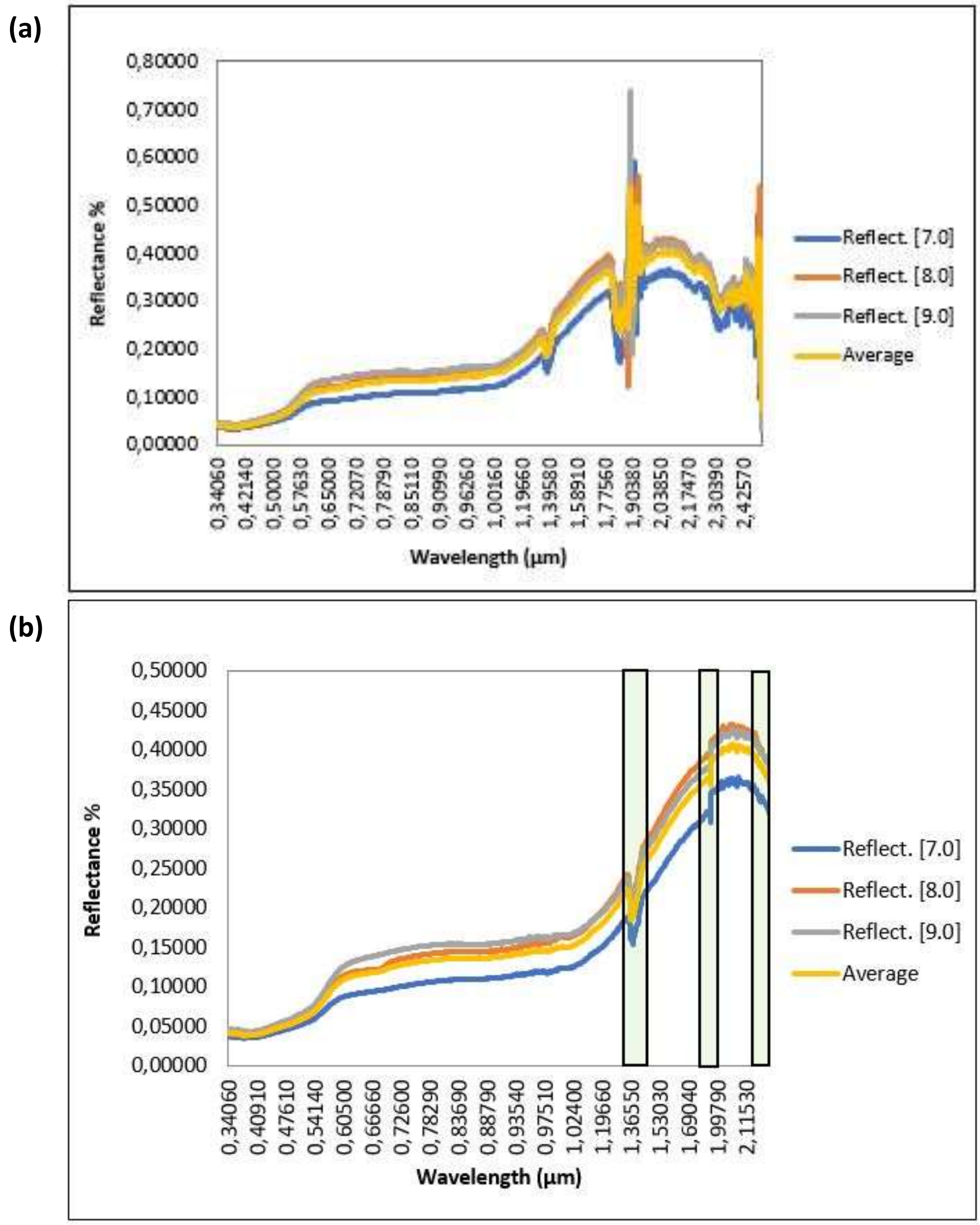

Figure 22: Reflectance Spectra of Metapelite: (a) Before Continuum Removal, (b) After Continuum Removal

Within the range of 0.4 to 2.2 µm, there is variability in the spectral reflectance of the metapeltic rocks of the Vredefort Dome. One of the noticeable features is the sharp absorption trough at 1.36 µm. The graph also shows a broad peak at around 2.80 µm, and on either side of that peak, there are two weak absorption troughs present at 1.81 µm and 2.20 µm respectively (Figure 22b). All of these features take place in the SWIR region.

All the visually interpreted diagnostic absorption features for each rock sample have been summarized in the table below (Table 4).

Table 4: Table Summarising the Diagnostic Absorption Bands of Rocks of the Vredefort Dome (Donkervleit area)

Rock Types	Diagnostic Absorption Features (µm)
Granite Gneiss	1312, 1856, 2210
Basalt	1384, 1849, 2325
Quartzite	1456, 1951, 2208
Meta-Ironstone	1373, 1965, 2210
Banded Iron Formation	1365, 1859, 2192
Metadolerite	1384, 1979, 2205
Metapelite	1369, 1811, 2208

4.3 Spectral library

Spectral signature curves are able to distinguish between the reflectance and emittance properties of targeted objects on the Earth's surface. It is these unique characteristics that allow us to differentiate between various features, just like human fingerprints can be used to tell us apart (Qaid and Basavarajappa, 2008). However, it should be noted that these spectral responses can be influenced by seasonality as well as other surface conditions; hence this study was conducted under controlled field conditions to minimize the effect of these external factors.

The large data values obtained from the spectroradiometer were converted to the same 10 m resolution as Sentinel-2 in order to create a spectral library (Figure 23) using ENVI software, which could be used as reference data for identifying and mapping the geology of the Donkervleit area in the Vredefort Dome. The results were then normalized using the continuum removal option under the analyst tools within the ENVI software. The normalization of the data was necessary in order to be able to directly compare the diagnostic absorption features from the collected reflectance spectrum of each representative rock sample (Clack, 1999; Van de Meer, 2000).

The outcomes of this normalisation show the 0.4 - 2.2 µm spectral range and as can be seen all the IR rock spectra have a fairly smooth appearance in the VIR region, followed by a major trough in the NIR region between 1.3-1.4 µm. According to literature, a dip in this region can be attributed to the presence of water vapour (Crowley *et al*., 2003; Skok *et al*., 2010).

The reflectance spectra then proceed to maintain a relatively smooth appearance as they progress into the SWIR region which is where we can see another noticeable dip at 2.2 µm for quartzite, granite gneiss, meta-ironstone and metadolerite. Metapelite, basalt and banded iron formation, on the other hand, seem to show an elevation in curvature around the same area as the previously mentioned rock types.

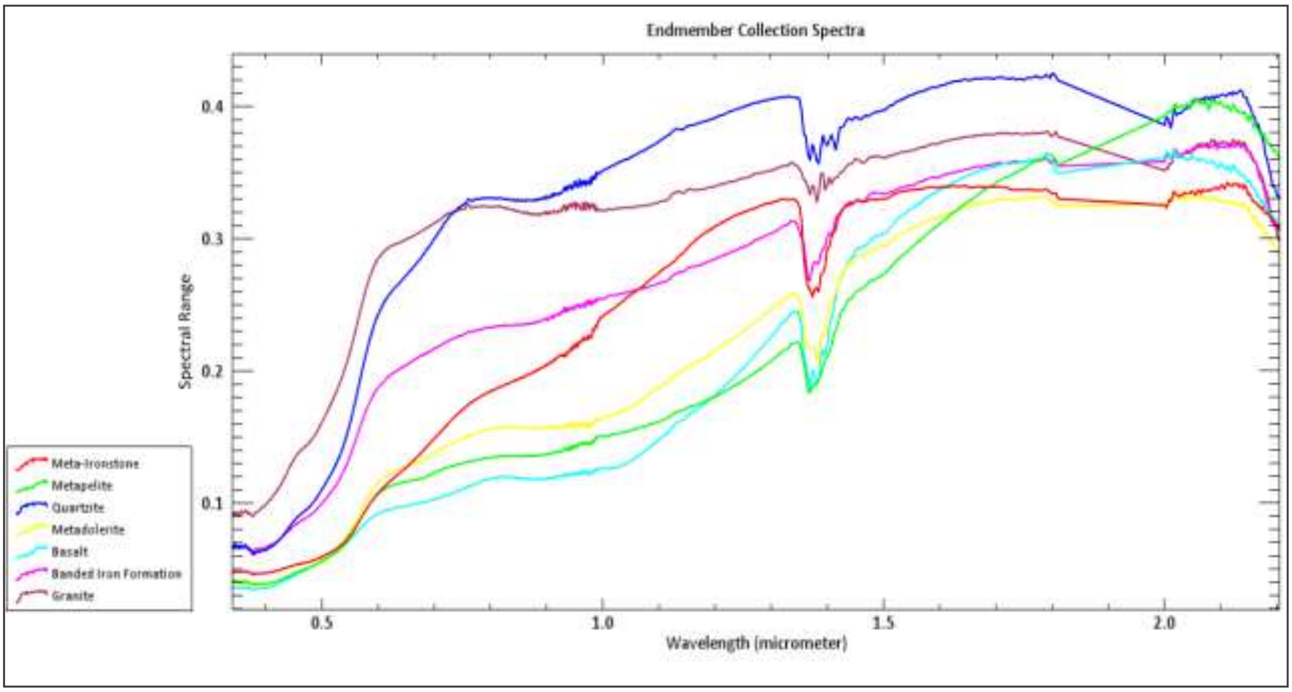

Figure 23: Spectral Library of the Rocks Collected in the Study Area

4.4 XRF Results

All rock types are made up of a varying combination of minerals with different chemical compositions which contribute towards the unique spectral signature of each rock type (Qaid and Basavarajappa, 2008). It is these variations we look for when trying to differentiate between the geology of a region. The X-ray fluorescence (XRF) technique was used to analyse the chemical makeup of each rock type and the results were displayed in Table 5.

Table 5: XRF Results

wt%	SiO_2	Al_2O_3	Fe_2O_3	FeO	MnO	MgO	CaO	Na_2O	K_2O	TiO_2	P_2O_5	Cr_2O_3	LOI	TOTAL
Meta-Ironstone	16.99	4.73	7.65	61.96	0.15	0.05	0.10	0.00	0.06	0.18	0.18	0.04	7.68	99.77
Metapelite	55.56	13.69	1.26	10.22	0.21	5.67	10.01	2.15	0.44	0.68	0.08	0.00	0.80	100.77
Quartzite	96.55	0.49	0.05	0.37	0.01	0.02	0.05	0.00	0.10	0.03	0.01	0.00	0.20	97.88
Metadolerite	54.42	13.47	1.06	8.59	0.17	8.38	9.92	2.34	0.12	0.73	0.15	0.11	0.68	100.14
Basalt	52.70	14.42	1.17	9.46	0.17	8.17	10.58	2.28	0.13	0.73	0.18	0.10	0.71	100.80
Banded Iron Formation (BIF)	63.63	19.29	0.77	6.19	0.04	4.21	0.39	1.15	1.99	0.87	0.06	0.12	1.50	100.21
Granite	73.47	13.95	0.18	1.42	0.03	0.25	1.03	4.22	3.74	0.18	0.14	0.00	0.79	99.40

4.5 Rock Identification and Map Generation

4.5.1 Rock Identification

The results from the NDVI analysis are shown in Figure 24. As can be observed from the RGB image the green areas are representative of the vegetation in the region. The RGB image was used to produce the NDVI image. In both the RGB image and the NDVI image, the pixel values for the vegetated areas was close to one which reflected as white in the NDVI image. The non-vegetated areas which symbolize the rock outcrops, built-up areas as well as the water bodies, have pixel values close to negative one which appeared as black (for the waterbodies) and varying shades of grey for all other objects in the area. This contrast in pixel values shades has led to their contrasting colours.

This contrast in pixel values along with the contrasting colours in the NDVI image allowed for the masking of the image. The results of the masking can be seen in Figure 25. The light blue regions are representative of the naturally occurring vegetation in the area, while the light brown areas are indicative of the cultivated land in the region. Once these areas were masked out, it made it easier to analyze the rock type variations in the area.

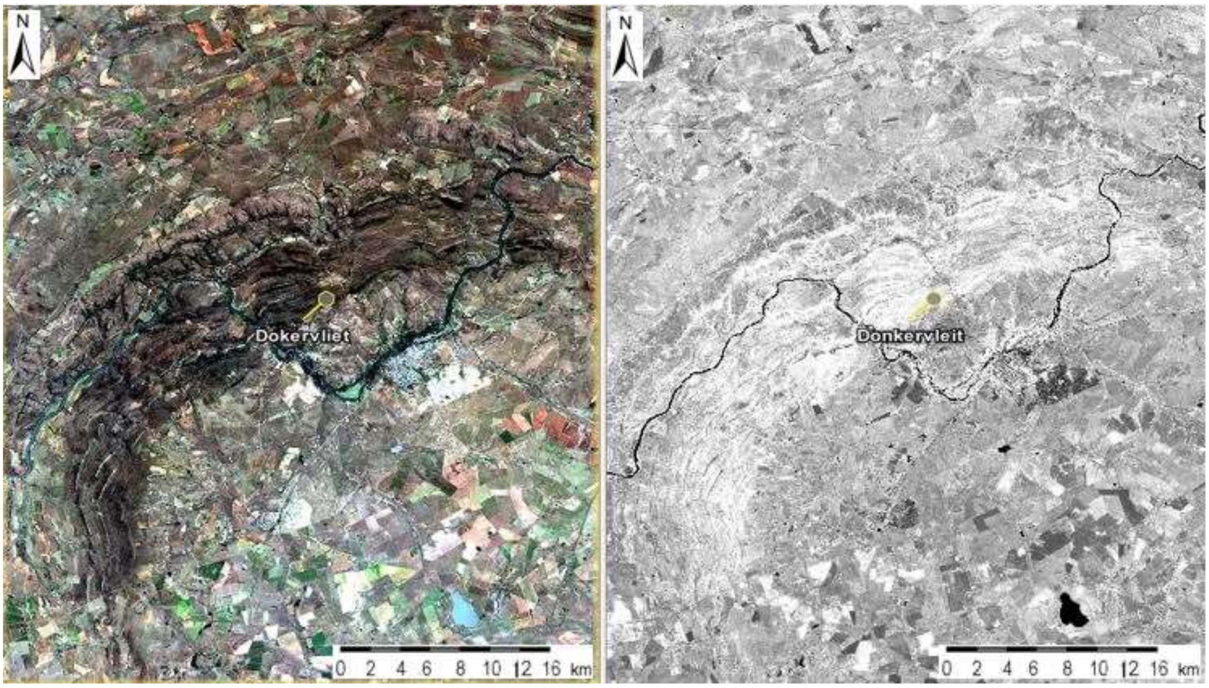

Figure 24: RGB Image (left) versus NDVI Image (right)

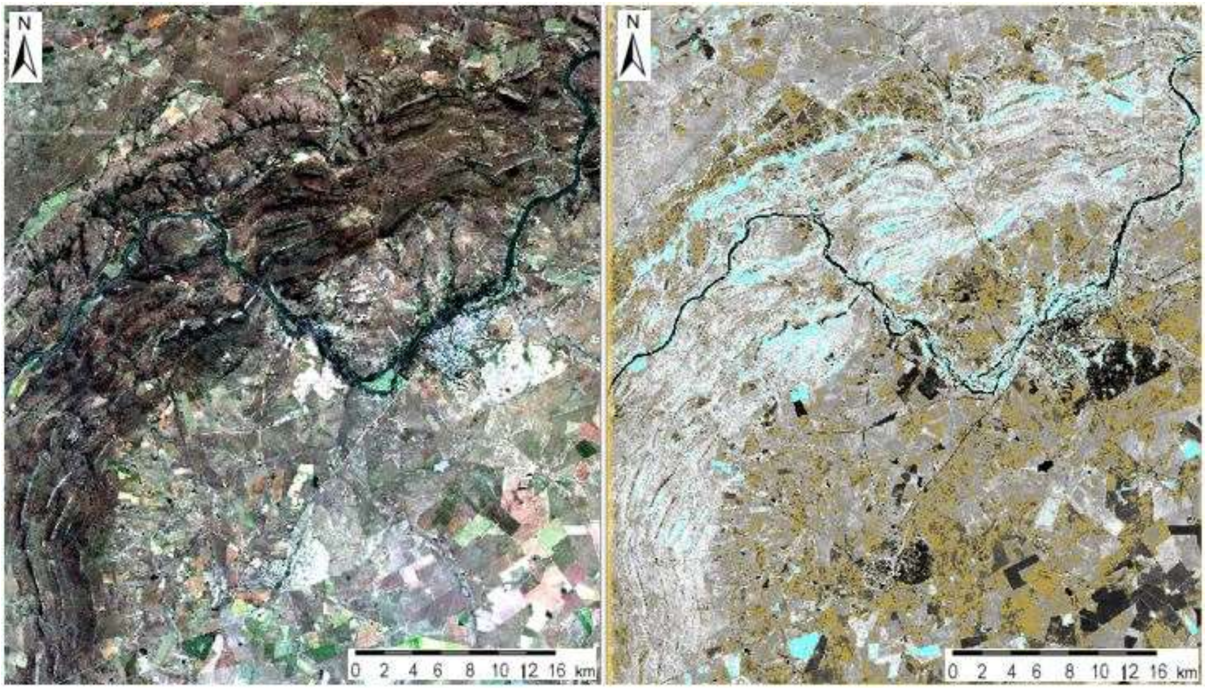

Figure 25: RGB Image (left) versus NDVI Masked Image (right)

4.5.2 Map Generation

The results as presented in Figure 26 showcase the outcomes of the mapping of the various rock types found in the geological study area. The Donkervleit area, which has never been observed/studied through the use of any other remote sensing instruments, was used. This area makes up a portion of the northern part of the Dome, and it was chosen because of its spatial extent as well as its gentle slopes which made general access to the area for purposes of data collection easier.

The major rock types found in the study area, in their stratigraphic order, from oldest to youngest, are granite gneiss, basalt, quartzite, meta-ironstone, banded iron formation (BIF), metadolerite and metapelite. Visual interpretation of the classified map revealed that granite gneiss, which forms the bedrock, followed by quartzite, which is predominantly found at the tops of the ridges, are two of the most abundant rock types occupying the study area. This can be attributed to the fact that these two rock types do not easily weather away (Goldich, 1938). Some of the rock types in the map registered as 'unclassified' due to the classification algorithm used not being able to place those rock types in any particular category.

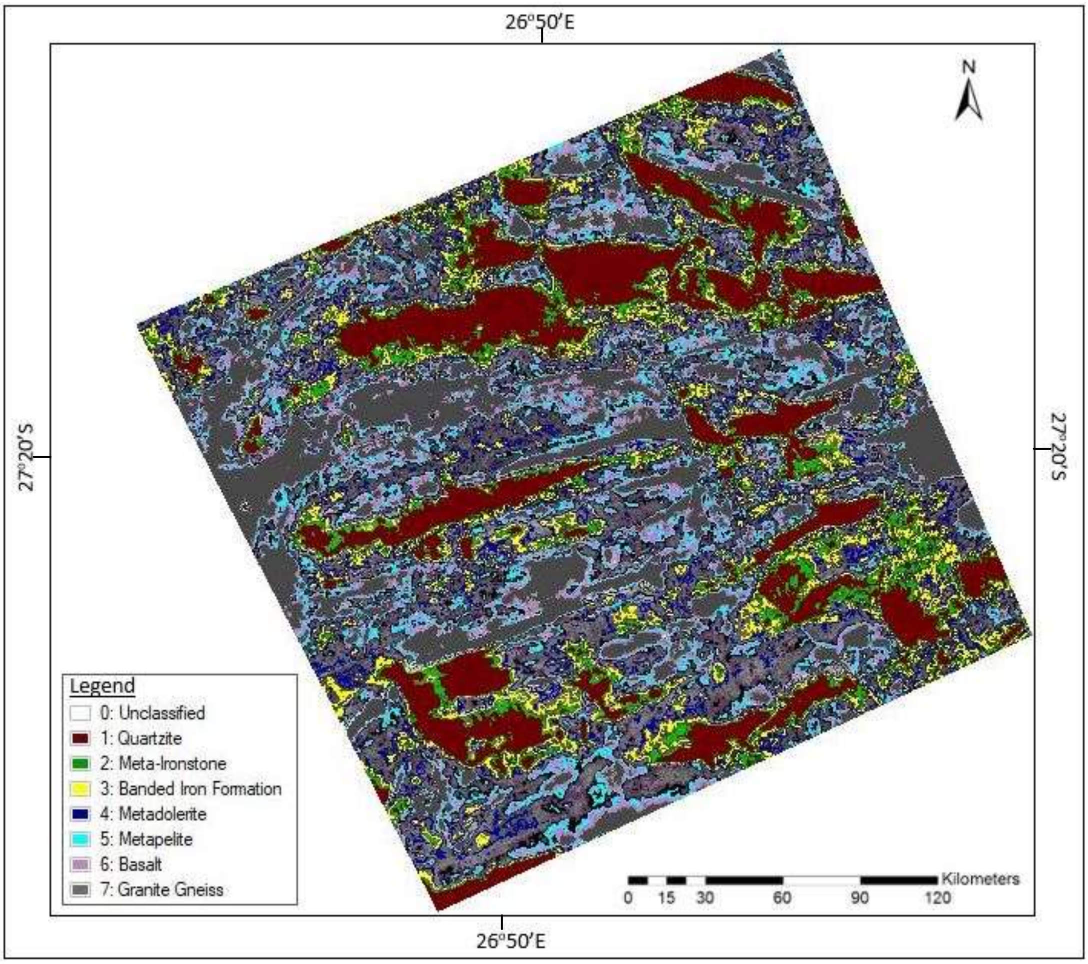

Figure 26: Classified Geological Map of the Study Area

4.5.3 Validation and Accuracy Assessment of the Results

The process of validation is used to determine the accuracy of the data under investigation (Tempfli *et al.*, 2009). In this study knowledgeable observations in linear transects that crossed the most variation over the shortest distance over the study area were made. Each rock type was observed at points located by photo-reading or GPS at pre-determined intervals of about 100m along the transect and then the predicted rock types were compared with the actual rock types and a classified map was produced (Figure 26). Once the validation of the results was done, the quality of the results had to be analysed and this required the selection of a sampling technique followed by the production of a confusion matrix which could be subsequently used to calculate the error parameters.

Table 6 shows the accuracy assessment results compiled using information from the selected ground truth ROIs. Training site data were collected by means of on-screen selection of polygonal training data method and the maximum number of training sites for the image were used in order to ensure that all spectral classes constituting each rock type were adequately represented in the training statistics. For each rock type 50 points were collected (35 training sites and 15 test sites). This process assigned each individual pixel in the image (based on its DN-values) to one of the predefined classes. It should be noted that the test and training site data which were initially split into 70% (training) and 30% (test) were combined in order to evaluate the overall accuracy. The results consist of the average user's accuracy, average producer's accuracy as well as the overall classification accuracy.

Key of classified/observed rock types:

Granite Gneiss	GG
Basalt	BA
Quartzite	QTZ
Meta-Ironstone	MI
Banded Iron Formation	BIF
Metadolerite	MD
Metapelite	MP

Table 6: Error Confusion Matrix Results

Classification	GG	BA	QTZ	MI	BIF	MD	MP	Row Total	Producer Accuracy (%)	Commission Results
GG	38	7	2	1	1	1	0	50	75	25
BA	5	44	1	0	0	0	0	50	86	14
QTZ	4	1	45	0	0	0	0	50	89	11
MI	0	0	3	40	5	1	1	50	81	19
BIF	0	0	1	6	39	2	2	50	78	22
MD	0	1	0	2	2	36	9	50	73	27
MP	1	2	0	2	3	7	35	50	71	29
Column Total	48	55	52	51	50	47	47	350		
User's Accuracy (%)	79.17	80.00	86.53	78.43	78.00	76.59	74.47			
Omission Results	20.83	20.00	13.47	21.57	22.00	23.41	25.53			

Overall Accuracy: 79%

Kappa Coefficient: 0.7625

Chapter 5: Discussion

One of the main purposes of this study was to describe and exploit the techniques related to the measurement and interpretation of the spectral signatures of the various rock types in the Vredefort region. The results were mainly derived from controlled field condition techniques applied to the collected samples which represent a variety of minerals and rocks found in the Vredefort study site. Having a basic knowledge of the spectral properties of objects, particularly minerals and rocks, and understanding the factors that influence the spectral response of the features of interest was required in order to properly apply the hands-on manipulations required for the aforementioned technique.

It can be seen from the results exhibited in this study that different spectral responses can be expected from different targeted objects due to the manner in which each object reacts when its energy is reflected or emitted over a variety of different wavelengths. Once these spectral responses are captured they can be used to distinguish and compare different features. For example, certain rock types may reflect similarly in the visible wavelengths but it becomes easier to distinguish between them in the infrared region.

Unfortunately, Hyperion had stopped tasking by the time this study was being conducted and that is one of the reasons why the mapping of the Vredefort Donkervleit area had to be conducted using Sentinel-2 imagery. In order to generate this map, reflectance values retrieved from the spectroradiometer had to be compared and up-scaled in order to match the reflectance values for the remotely sensed image.

Looking at the outcomes of the confusion matrix (Tables 6), it can be seen that the commission and omission errors for metadolerite and metapelite are among the highest; this is mainly due to the spectral similarities between these two rock types. Even from the XRF results in Table 5, it can be seen that metadolerite and metapelite possesses very similar elemental compositions. The biggest difference could be observed between the quartzite and basalt because of their non-overlapping mineral compositions.

The Kappa coefficient, which may be used as a measure of agreement between classified images and reality, was also calculated. Kappa values usually range between zero and one; where one is representative of the image being 100% correctly classified while zero represents complete randomness, meaning there is no correlation between the classified image and the reference data. The Kappa result for this classification was 0.7625.

Also, based on the validation and accuracy results of the classified map it can be seen that there is a moderate agreement between the ground truthing results and the mapped out results but a 79% accuracy does not fully meet the minimum frequency for classification accuracy which is usually considered to be higher than 85% (Aronoff, S., 1982; Congalton, 1991; Congalton and Green, 2008). This has led to the conclusion that Sentinel-2 is not necessarily the best sensor to use in the pursuit to identify geological structures when compared to other multispectral sensors such as Aster and Landsat which have been known to produce accuracies between 82% - 92% (Zhang and Pazner, 2007; Zhang *et al.*, 2007, Yu *et al*., 2012).

Chapter 6: Conclusions, Limitations and Recommendations

6.1 Conclusion

Until the last decade, the field of geological mapping using spectroscopy was largely unexplored, mainly because of the notorious difficulty in generating and detecting the respective minerals. Every rock type has a unique spectral response to electromagnetic radiation due to their varying crystal structures and chemical compositions, which can be picked up in satellite imagery and be used in the identification and mapping of exposed rock types (Tempfli *et al.*, 2009; Gupta, 2013). The problem with this is that the precision and accuracy with which these rocks can be classified is dependent on the reflectance spectra of each of their minerals as well as the type of sensor used; thus, making it crucial to determine which satellite images are most suitable for this task and how much precision they can offer (Tempfli *et al.*, 2009; Gupta, 2013).

In this particular study spectral data was collected using controlled field-based methods in conjunction with Sentinel-2 satellite data. The spectral data was used to create a spectral library and it was also used as reference data in order to select the relevant pixels in the satellite imagery. The results obtained from this study showed that controlled field-based procedures carried out using a spectroradiometer can be quite effective at capturing spectral signatures of targeted surfaces and that ENVI software can be a very useful spectral data processing tool. Unfortunately, it was also through this study that it was discovered that Sentinel-2 satellite imagery is not the best at lithological identification and was only able to produce a classification accuracy of 79%, which is reasonably accurate but other sensors such as Landsat and Aster have been known to produce maps of higher accuracy that range between 82% - 92%.

6.1.1 Aims and Objectives Reviewed

This study aimed to evaluate whether field-based techniques in conjunction with Sentinel-2 imagery could be used to identify and map out the geology of the Vredefort Dome. This was achieved by carrying out the following objectives:

- **Capture and process the spectral signatures of the rocks found in the study area.**

In order to fulfil this objective, rock samples had to be carefully removed from the study area and brought back into a controlled environment which mimicked their original environment and allowed for easier capturing of the spectral signatures of the samples through the use of a handheld spectroradiometer (Spectral Evolution). A minimum of three measurements were collected from various locations on each sample so as to account for the variability in the mineralogy as well as the surface roughness of each rock type.

- **Create a spectral library using the collected spectral signatures.**

Once the spectral signatures were captured, these results were then processed using the relevant software (ENVI and SNAP) in order to create a spectral library of the rocks present in the study area. This spectral library could be used to identify the absorption features of each rock type but only once the continuum removal technique had been applied.

- **Identify and map the different rock types that make up the study area.**

The collected rock samples were turned into powdery substances, using crushing and milling equipment in the geosciences lab. Each powdery substance was individually packaged, clearly marked and sent through to a laboratory for XRF analysis. The results from the XRF showed the major elemental composition of each rock type which was then used to accurately identify the samples and match them to their GPS coordinates. For visualization and interpretation purposes, the acquired Sentinel-2 sub-scene was atmospherically corrected, rectified to a common UTM coordinate system and its suitable bands required for a geological study were identified. The vegetation in the area also had to be masked out in order to focus solely on the classification and mapping out of the spatial distribution of the rocks present in the study area.

- **Assess how accurately Sentinel-2 was able to map out the geology of the study area.**

For each rock type, 50 points were collected (35 training sites and 15 test sites) and using ENVI's post-classification option, a confusion matrix consisting of the producer, user and overall accuracy was created in order to see how accurately Sentinel-2 imagery could be used to identify and map out the geology of the region of interest.

6.2 Limitations and Recommendations

This study was able to show that there are significant spectral differences between the metamorphic rocks present in the Vredefort Dome when using a spectroradiometer. However, when looking at the map produced from the obtained satellite imagery data, it can be seen that Sentinel-2, according to scientific standards, is not adequately able to identify the geology of a particular region due to the fact that it was only able to produce a map with a 79% accuracy while other multispectral sensors have been known to produce accuracy levels as high as 95%.

This, however, was anticipated due to the fact that literature from the likes of Kumar *et al.* (2013), Van der Meer *et al.* (2014) and Yokoya *et al.* (2016), had previously suggested that Sentinel-2 had been created with the sole purpose of monitoring plant growth, meaning that in the developmental stages of this satellite, mineral identification was not prioritized. This implies that factors such as which sensor to use for a particular study, need to always be considered when using imagery as an exploration or mapping tool.

This has led to the conclusion that Sentinel-2 is not the most appropriate multispectral sensor to use for geological mapping and that a different sensor be used, preferably Hyperion or ASTER, which are more accurately able to be used for mapping out rock distributions.

Other issues that arose are that the spectroradiometer could only be used under direct sunlight in order to obtain the most accurate results and only prominent outcrops could be used because the rocks had to be both visually and spectrally identifiable in the satellite images. Also, there are areas of the Vredefort Dome that are heavily vegetated as well as fenced off, which make it difficult to access for ground-truthing purposes but since the geology of the Vredefort Dome is already well documented, it would be worthwhile for future remote sensing studies in the region to focus on trying to infer the geology from the type of vegetation present in the area. This, however, would require the combined knowledge of both remote sensing and geo-botany.

Creating an open-source spectral signature database that all relevant parties can access and contribute to would also be beneficial for the advancement of this discipline. However, this would have to go beyond the scope of the chosen study area, primarily due to the fact that the Vredefort Dome is a protected World Heritage Site, which may make it difficult to obtain all the relevant data required. Furthermore, South Africa is a country that is heavily dependent on its mining industry and most activities channelled toward identifying the geology of a particular region are done with the main purpose of identifying precious minerals such as platinum and gold.

Lastly, it should be noted that more in-depth spectral analysis can be performed in the Vredefort Dome region by performing other techniques such as applying a multi-linear regression to the absorption band parameters (Van der Meer, 2004). However, most of these in-depth spectral analysis techniques will require one to possess a great deal of knowledge and experience in the field of spectroscopy.

References

AccuWeather.com (2018). Weather: Vredefort. Available from (Accessed 28/06/2018): https://www.accuweather.com/en/za/vredefort/297879/june-weather/297879?year=2018

Amrutkar, R., Parakh, K., Chudasama, B., Thakur, S., Aranha, M., and Porwal, A., (2016). Laboratory based, field-based, and satellite-borne spectroscopy for lithological discrimination. In *Society of Photo-Optical Instrumentation Engineers (SPIE), Conference Series*, 9880, 1-8.

Anbazhagan, S. and Arivazhagan, S., (2010). Reflectance spectra of analog anorthosites: Implications for lunar highland mapping. *Planetary and Space Science*, 58(5), 752 760.

Aronoff, S., (1982). Classification accuracy: a user approach. *Photogrammetric Engineering and Remote Sensing*, 48(8), 1299-1307.

Baldridge, A. M., Hook, S. J., Grove, C. I., and Rivera, G., (2009). The ASTER spectral library version 2.0. *Remote Sensing of Environment*, 113(4), 711-715.

Bertel, L., Deronde, B., Fernandez, M., Kempeneers, P., Knaeps, E., Meuleman, K., Reusen, I., Ruddick, K., Sterckx, S., Trefois, P. and Mol, V., (2006). The spectral signatures of minerals and rocks. *Hyperteach: Training in imaging spectroscopy*. AFRICAN SUN MeDia, Stellenbosch, 42-48.

Borengasser, M., Hungate, W. S., and Watkins, R., (2007). Information Extraction from Optical Image Data. In *Hyperspectral remote sensing: principles and applications.* CRC Press, Boca Raton, 39-55.

Bourgeois, J., and Koppes, S., (1998). Robert S. Dietz and the Recognition of Impact Structures on Earth. *Earth Sciences History*, *17*(2), 139-156.

Bredenkamp, G.J., and Van Rooyen, N., (1996). Rocky Highveld Grassland. In *Vegetation of South Africa, Lesotho and Swaziland*. Department of Environmental Affairs & Tourism, Pretoria, 39.

Chen, K., Kunz, M., Tamura, N. and Wenk, H.R., (2011). Evidence for high stress in quartz from the impact site of Vredefort, South Africa. *European Journal of Mineralogy*, 23, 169–178.

Clark, R.N. (1999). Spectroscopy of Rocks and Minerals, and Principles of Spectroscopy. *Manual of Remote Sensing*, U.S. Geological Survey, Denver, 3, 3-58.

Clark, R.N., Swayze, G.A., Wise, R., Livo, K.E., Hoefen, T., Kokaly, R.F. and Sutley, S.J., 2007. USGS digital spectral library splib06a (No. 231). Digital Data Series, U.S. Geological Survey, Reston.

Climate-Data.org, (2012). Climate: Vredefort. Available from (Accessed 23/07/2018): https://en.climatedata.org/location/27405/

Congalton, R. G., (1991). A review of assessing the accuracy of classifications of remotely sensed data. *Remote densing of Environ*ment, 37(1), 35-46.

Congalton, R.G. and Green, K., (2008). In *Assessing the accuracy of remotely sensed data: principles and practices*. CRC press, Boca Raton, 55-59, 105-119.

Conradie, W., (2006). *Seasonal variation in anuran diversity and activity in the Vredefort Dome conservation area* (Doctoral dissertation, North-West University).

Cracknell, M. J. and Reading, A. M., (2014). Geological mapping using remote sensing data: A comparison of five machine learning algorithms, their response to variations in the spatial distribution of training data and the use of explicit spatial information. *Computers & Geosciences* (63), 22-33.

Crowley, J.K., Williams, D.E., Hammarstrom, J.M., Piatak, N., Chou, I.M. and Mars, J.C., (2003). Spectral reflectance properties (0.4–2.5 μm) of secondary Fe-oxide, Fe hydroxide, and Fe-sulphate-hydrate minerals associated with sulphide-bearing mine wastes. *Geochemistry: Exploration, Environment, Analysis*, *3*(3), 219-228.

Debba, P., van Ruitenbeek, F.J.A., van der Meer, F.D., Carranza, E.J.M. and Stein, A. (2005). Optimal field sampling for targeting minerals using hyperspectral data. *Remote Sensing of Environment*, 99, 373-386.

De Carvalho, O. A., and Meneses, P. R., (2000). Spectral correlation mapper (SCM): an improvement on the spectral angle mapper (SAM). In *Summaries of the 9th JPL Airborne Earth Science Workshop, JPL Publication 00-18* (Vol. 9). JPL Publication, Pasadena, CA.

Drusch, M., Del Bello, U., Carlier, S., Colin, O., Fernandez, V., Gascon, F., Hoersch, B., Isola, C., Laberinti, P., Martimort, P. and Meygret, A., (2012). Sentinel-2: ESA's optical high resolution mission for GMES operational services. *Remote sensing of Environment*, *120*, 25-36.

Dumke, I. and Teschner, M., (1988). Application of fluorescence spectroscopy to geochemical correlation problems. *Organic Geochemistry*, *13*(4), 1067-1072.

Elipe, M.V.S., (2003). Advantages and disadvantages of nuclear magnetic resonance spectroscopy as a hyphenated technique. *Analytica Chimica Acta*, 497(1-2), 1-25.

Flowers, R.M., Moser, D.E. and Hart, R.J., (2003). Evolution of the amphibolite-granulite facies transition exposed by the Vredefort impact structure, Kaapvaal Craton, South Africa. *Journal of Geology*, 111, 455–470.

Frampton, W.J., Dash, J., Watmough, G. and Milton, E.J., (2013). Evaluating the capabilities of Sentinel-2 for quantitative estimation of biophysical variables in vegetation. *ISPRS Journal of Photogrammetry and Remote Sensing*, *82*, 83-92.

Ge, W., Cheng, Q., Jing, L., Armenakis, C. and Ding, H., (2018). Lithological discrimination using ASTER and Sentinel-2A in the Shibanjing ophiolite complex of Beishan orogenic in Inner Mongolia, China. *Advances in Space Research*, *62*(7), 1702-1716.

Gibson, R.L. and Reimold, W.U., (2008). *Geology of the Vredefort impact structure: A guide to sites of interest.* Memoir of the Council for Geoscience, 97.

Girouard, G., Bannari, A., El Harti, A., and Desrochers, A., (2004). Validated spectral angle mapper algorithm for geological mapping: comparative study between QuickBird and Landsat-TM. In *XXth ISPRS Congress*, *Geo-Imagery Bridging Continents*, Istanbul, Turkey, 12-23.

Goldich, S.S., (1938). A study in rock-weathering. *The Journal of Geology*, 46(1), 17-58.

Grieve, R.A., Reimold, W. U., Morgan, J., Riller, U., and Pilkington, M., (2008). Observations and interpretations at Vredefort, Sudbury, and Chicxulub: Towards an empirical model of terrestrial impact basin formation. *Meteoritics & Planetary Science*, *43*(5), 855-882.

Gupta, R. P., (2013). *Remote Sensing Geology*. Springer Science & Business Media. Immitzer, M., Vuolo, F. and Atzberger, C., (2016). First experience with Sentinel-2 data for crop and tree species classifications in central Europe. *Remote Sensing*, *8*(3), 166.

Ivanov, B., (2008). Geologic effects of large terrestrial impact crater formation. *Catastrophic Events Caused by Cosmic Objects*, 163. 17

Hunt G.R., (1980). Electromagnetic radiation: the communication link in remote sensing. In Siegel B.S., Gillespie A.R. (eds), *Remote Sensing in Geology*. John Wiley & Sons, New York, USA, 5-45.

Hunt G.R. and Salisbury J.W., (1970). Visible and near infrared spectra of minerals and rocks: I Silicate minerals*. Modern Geology*, *1,* 283-300.

Hunt G.R. and Salisbury J.W. and Lenhoff C.J., (1973). Visible and near-infrared spectra of minerals and rocks: VII Acidic igneous rocks*. Modern Geology*, 4, 217-224.

Jehlička, J., Urban, O. and Pokorný, J., (2003). Raman spectroscopy of carbon and solid bitumens in sedimentary and metamorphic rocks. *Spectrochimica Acta Part A: Molecular and Biomolecular Spectroscopy*, 59(10), 2341-2352.

Kaplan, G. and Avdan, U., (2017). Object-based water body extraction model using Sentinel-2 satellite imagery. *European Journal of Remote Sensing*, *50*(1), 137-143.

Kottek, M., Grieser, J., Beck, C., Rudolf, B., and Rubel, F., (2006). World map of the Köppen-Geiger climate classification updated. *Meteorologische Zeitschrift*, *15*(3), 259-263.

Kruse, F.A., and Perry, S.L., (2009). Improving multispectral mapping by spectral modelling with hyperspectral signatures. *Journal of Applied Remote Sensing*, 3(1), 1931-1959.

Kruse, F.A., (2012). Mapping surface mineralogy using imaging spectrometry*. Geomorphology*, 137(1), 41-56.

Kuester, M., Thome, K., Krause, K., Canham, K. and Whittington, E., (2001). Comparison of surface reflectance measurements from three ASD FieldSpec FR spectroradiometers and one ASD FieldSpec VNIR spectroradiometer. In *IGARSS 2001. Scanning the Present and Resolving the Future. Proceedings. IEEE 2001 International Geoscience and Remote Sensing Symposium (Cat. No. 01CH37217),* 1, 72-74.

Kumar, S.S., Arivazhagan, S., and Rangarajan, N. (2013). Remote Sensing and GIS Applications in Environmental Sciences – A Review. *Journal of Environmental Nanotechnology*, *2*(2), 92-101.

Lana, C., Gibson, R.L., and Reimold, W.U., (2003). Impact tectonics in the core of the Vredefort dome, South Africa: Implications for central uplift formation in very large impact structures. *Meteoritics & Planetary Science*, *38*(7), 1093-1107.

Lieger, D., Riller, U. and Gibson, R.L. 2009. Generation of fragment-rich pseudotachylite bodies during central uplift formation in the Vredefort impact structure, South Africa. *Earth and Planetary Science Letters*, 279, 53–64.

Longhi, I., Sgavetti, M., Chiari, R. and Mazzoli, C., (2001). Spectral analysis and classification of metamorphic rocks from laboratory reflectance spectra in the 0.4-2.5 μm interval: A tool for hyperspectral data interpretation. *International Journal of Remote Sensing*, *22*(18), 3763-3782.

Martimort, P., Fernandez, V., Kirschner, V., Isola, C. and Meygret, A., (2012). Sentinel-2 MultiSpectral imager (MSI) and calibration/validation. In *The 2012 IEEE International Geoscience and Remote Sensing Symposium,* IEEE, Munich, Germany, 6999-7002.

Marvin, U.B., (1999). Impacts from space: the implications for uniformitarian geology. *Geological Society, London, Special Publications*, *150*(1), 89-117.

McCoy, R.M., (2005). *Field methods in remote sensing*. Guilford Press, New York.

Miyashiro A., (2012). *Metamorphism and Metamorphic Belts*. The Gresham Press, Old Woking, Surrey.

Mustard, J.F. and Sunshine, J.M., (1999). Spectral analysis for earth science: investigations using remote sensing data. *Remote sensing for the earth sciences: Manual of Remote Sensing*, 3, 251-307.

Nesse, W.D., (2009). *Introduction to Minerology*. Oxford University Press, New York.

Ngcofe, L., and Van Niekerk, A., (2016). Advances in optical earth observation for geological mapping: A Review. *South African Journal of Geomatics*, CONSAS, Rondebosch, 5(1), 1-16.

Parakh, K., Thakur, S., Chudasama, B., Tirodkar, S., Porwal, A., and Bhattacharya, A., (2016). Machine learning and spectral techniques for lithological classification. In *Society of Photo-Optical Instrumentation Engineers (SPIE), Conference Series*, 9880, 1-12.

Pour, A.B., Park, Y., Park, T.Y.S., Hong, J.K., Hashim, M., Woo, J. and Ayoobi, I., (2018). Regional geology mapping using satellite-based remote sensing approach in Northern Victoria Land, Antarctica. *Polar Science*, 16, 23-46.

Qaid, A.M. and Basavarajappa, H.T., 2008. Integration of Geological, Geochemistry and Remote Sensing data for evolution of the Precambrian rocks, north east of Hajjah, Republic of Yemen. *Journal of Applied Geochemistry*, 10, 76-91.

Reimold, W.U. and Gibson, R.L., (2010). *Meteorite Impact!: The Danger from Space and South Africa's Mega-Impact The Vredefort Structure* (Vol. 1). Springer, Heidelberg.

Reimond, W.U., and Koeberl, C., (2014). Impact Structures in Africa: A review. *Journal of African Earth Sciences*, 93, 57-175.

Sabins, F.F., (1999). Remote sensing for mineral exploration. *Ore Geology Reviews*, 14(3-4), 157-183.

Santos, M.C., Morais, C.L., Nascimento, Y.M., Araujo, J.M. and Lima, K.M., (2017). Spectroscopy with computational analysis in virological studies: A decade (2006 2016). *TrAC Trends in Analytical Chemistry*, 97, 44-256.

Sgavetti, M., Pompilio, L. and Meli, S. (2006). Reflectance spectroscopy (0.3-2.5µm) at various scales for bulk-rock identification, *Geosphere*, 2(3), 142-160.

Shaw, G.A. and Burke, H.K., (2003). Spectral imaging for remote sensing. *Lincoln laboratory Journal*, Massachusetts Institute of Technology, Lexington, 14(1), 3-28.

Simpson, C., De Paor, D.G., Beebe, M.R., and Strand, J.M., (2012). Transferring maps and data from pre-digital era theses to Google Earth: A case study from the Vredefort Dome, South Africa. In *Google Earth and Virtual Visualizations in Geoscience Education and Research.* Geological Society of America Special Papers, Colorado, 492, *183-197.*

Smith, R.B., (2012). Introduction to hyperspectral imaging. Available from (Accessed 11/04/2018): https://www.microimages.com/documentation/Tutorials/hyprspec/

Skok, J.R., Mustard, J.F., Ehlmann, B.L., Milliken, R.E., and Murchie, S.L., (2010). Silica deposits in the Nili Patera caldera on the Syrtis Major volcanic complex on Mars. *Nature Geoscience*, *3*(12), 838-841.

spectralevolution.com, (2004). Products: Field Portable Spectroradiometers for Remote Sensing. Available from (Accessed 15/10/2018): https://spectralevolution.com/products/hardware/field-portablespectroradiometer-for-remote-sensing/

Stephens, D.C., Leggett, S.K., Cushing, M.C., Marley, M.S., Saumon, D., Geballe, T.R., Golimowski, D.A., Fan, X. and Noll, K.S., (2009). The 0.8-14.5 μm spectra of mid-L to mid-T dwarfs: Diagnostics of effective temperature, grain sedimentation, gas transport, and surface gravity. *The Astrophysical Journal*, *702*(1), 154.

Stepto, D., (1979). *A geological and geophysical study of the central portion of the Vredefort Dome Structure.* PhD Dissertation (unpublished), University of the Witwatersrand, Johannesburg, South Africa.

Stepto, D., (1990). The geology and gravity field in the central core of the Vredefort structure. *Tectonophysics*, 171(1-4), 75-103.

Tempfli, K., Huurneman, G., Bakker, W., Janssen, L., Bakker, W.H., Feringa, W.F., Gieske, A.S.M., Grabmaier, K.A., Hecker, C.A., Horn, J.A. and Huurneman, G.C., (2009). *Principles of Remote Sensing: an Introductory Textbook*. ITC, the Netherlands.

Therriault, A.M., Grieve, R.A.F. and Reimold, W.U., (1997). Original size of the Vredefort Structure, South Africa. *Meteoritics & Planetary Science*, 32, 71–77.

Toselli, F. and Bodechtel, J. eds., (1991). *Imaging spectroscopy: fundamentals and prospective applications* (Vol. 2). Springer Science & Business Media.

Van Der Meer, F., (2000). Spectral curve shape matching with a continuum removed CCSM algorithm. *International Journal of Remote Sensing*, 21(16), 3179-3185.

Van der Meer, F.D. and De Jong, S.M. eds., (2011). *Imaging spectrometry: basic principles and prospective applications* (Vol. 4). Springer Science & Business Media, Dordrecht, Netherlands.

Van der Meer, F.D., Van der Werff, H.M.A., and Van Ruitenbeek, F.J.A., (2014). Potential of ESA's Sentinel-2 for geological applications. *Remote Sensing of Environment*, 148, 124-133.

Walt, I.J., Pretorius, S.J., and Schoeman, C.B., (2010). The role of geohydrology in the determination of a spatial development framework in the Vredefort dome world heritage site. *Water*, *2*(4), 742-772.

Wårell, L., (2007). A horizontal merger in the iron ore industry: An event study approach. *Resources Policy*, 32(4), 191-204.

Wieland, F., Gibson, R.L. and Reimold, W.U., (2005). Structural analysis of the collar of the Vredefort Dome, South Africa – Significance for impact-related deformation and central uplift formation*. Meteoritics & Planetary Science*, 40, 1537–1554.

Yokoya, N., Chan, J.C.W., and Segl, K., (2016). Potential of resolution-enhanced hyperspectral data for mineral mapping using simulated EnMAP and Sentinel-2 images. *Remote Sensing*, 8(3), 172-190.

Yu, L., Porwal, A., Holden, E.J., and Dentith, M.C., (2012). Towards automatic lithological classification from remote sensing data using support vector machines. *Computers & Geosciences*, (45), 229-239.

Zhang, X. and Pazner, M., (2007). Comparison of lithologic mapping with ASTER, Hyperion, and ETM data in the southeastern Chocolate Mountains, USA. *Photogrammetric Engineering & Remote Sensing*, *73*(5), 555-561.

Zhang, X., Pazner, M. and Duke, N., (2007). Lithologic and mineral information extraction for gold exploration using ASTER data in the south Chocolate Mountains (California). *ISPRS Journal of Photogrammetry and Remote Sensing*, *62*(4), 271-282.

448251:Bogatsu_Mpho.pdf

ORIGINALITY REPORT

3%	0%	0%	3%
SIMILARITY INDEX	INTERNET SOURCES	PUBLICATIONS	STUDENT PAPERS

PRIMARY SOURCES

1	Submitted to University of Witwatersrand Student Paper	3%

Exclude quotes	On	Exclude matches	< 2%
Exclude bibliography	On		